Supplementary Information (SI) for Journal of Materials Chemistry C.
This journal is © The Royal Society of Chemistry 2025

Supporting information for:

Multistate emission of TICT luminophores

Marek P. Szymański,[a†] Agnieszka Czapik,[b†] Marzena Banasiewicz,[c] Klaudia Chuchracka,[b] Marcin Kwit,[b] Agnieszka Szumna*[a] and Paweł Skowronek*[b]

[a.] *Institute of Organic Chemistry, Polish Academy of Sciences, Kasprzaka 44/52, 01-224 Warsaw, Poland. E-mail: agnieszka.szumna@icho.edu.pl.*
[b.] *Faculty of Chemistry, Adam Mickiewicz University, Uniwersytetu Poznanskiego 8, 61-614 Poznań, Poland. E-mail: pawel.skowronek@amu.edu.pl*
[c.] *Institute of Physics, Polish Academy of Sciences, Aleja Lotników 32/46, 02-668 Warsaw, Poland.*

Table of contents:

Synthesis and analytical characterization

Substrate availability and analytical characterization

- 2,5-Dibromoterephtalaldehyde was obtained according to the previously described procedure.[1]
- 4-(*N*,*N*'-Dimethylamino)phenylboronic acid was purchased from BLDpharm.
- 4-(*N*,*N*'-diphenylamino)phenylboronic acid from Angene.
- 2-bromobenzaldehyde from Fluorochem
- Catalysts $Pd(PPh_3)_4$ and $Pd(OAc)_2$ from Merck.

^1H and ^{13}C NMR spectra were recorded on a Bruker 600 MHz at ambient temperature. All ^1H NMR spectra are reported in parts per million (ppm) downfield of TMS and were measured relative to the signals for TMS. All ^{13}C NMR spectra were reported in ppm relative to residual $CDCl_3$ (77.0 ppm) and were obtained with ^1H decoupling.

2,5-di(4-(*N*,*N*'-diphenylamino)phenyl)terephtalaldehyde (1)[2]

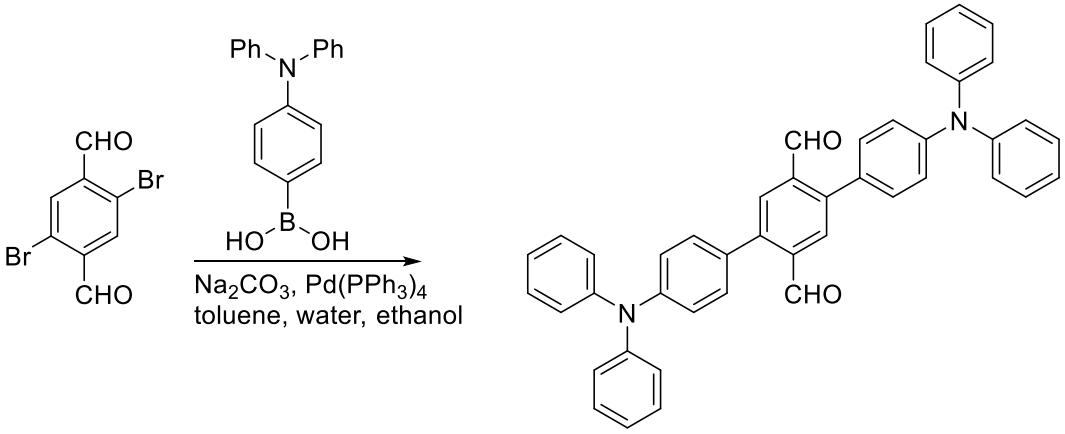

(4-(Diphenylamino)phenyl)boronic acid (3 g, 10.3 mmol) and sodium carbonate (1.1 g, 10.3 mmol) were dissolved in deionized water. To this solution, 2,5-dibromoterephthalaldehyde (1.06 g, 3.5 mmol) and anhydrous ethanol were added. The mixture was stirred and heated (60 °C) under an argon atmosphere. A solution of $Pd(PPh_3)_4$ (0.11 g, 0.1 mmol) in anhydrous toluene was then added, and the reaction was heated to 90 °C with stirring for two days. After the mixture was cooled to room temperature, dichloromethane (DCM) and water were added. The organic layer was separated, dried over anhydrous Na_2SO_4, and the solvent was removed by evaporation. The crude product was purified by column chromatography on silica gel, using a mixture of DCM:hexane (*v*:*v*, 2:1) containing triethylamine (Et_3N, 1%) as the eluent. The product-containing fractions were combined, and the solvent was evaporated. The solid residue was crystallized from chloroform and washed with diethyl ether to yield the final product as a yellow solid (70% yield).

Spectral data are identical to those previously reported.[2]

^{1}H NMR (600 MHz, $CDCl_3$) δ 10.16 (s, 1H), 8.09 (s, 1H), 7.34–7.29 (m, 4H), 7.26 (m, 2H), 7.19–7.15 (m, 6H), 7.09 (m, 2H).

^{13}C NMR (151 MHz, $CDCl_3$) δ 192.14, 148.48, 147.22, 143.76, 136.44, 130.91, 130.10, 129.48, 125.05, 123.68, 122.40.

2,5-di(4-(*N*,*N*'-dimethylamino)phenyl)terephtalaldehyde (2)[3]

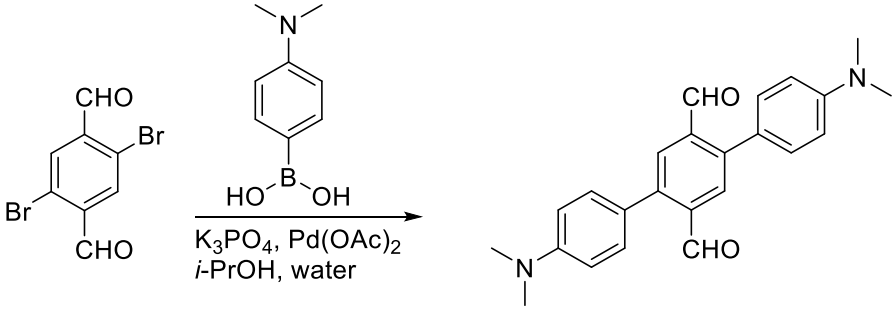

2,5-Dibromoterephthalaldehyde (291 mg, 1 mmol) was dispersed in isopropanol (12 mL). To this stirred mixture, 4-(N,N-dimethylamino)phenylboronic acid (363 mg, 2.2 mmol) was added, followed by a solution of $K_3PO_4 \cdot 3H_2O$ (913 mg, 4 mmol) in distilled water (4 mL). Next, palladium(II) acetate (6.7 mg, 0.03 mmol) was added. The mixture, which turned red, was placed in an oil bath preheated to 80 °C and was heated for 4 hours. After this time, the mixture was cooled, and brine (15 mL) was added. The reaction mixture was extracted with dichloromethane. The dark red organic solution was dried over anhydrous Na_2SO_4 and filtered through a pad of silica gel. After evaporation of the solvents, the crude red product was obtained (321 mg, 86% yield). The crude product was then crystallized from toluene to yield the final product as red needles (256 mg, 68% yield).

Spectral data are identical to those previously published.[4]

^{1}H NMR (600 MHz, $CDCl_3$) δ 10.10 (s, 1H), 8.06 (s, 1H), 7.31 (d, J = 8.8 Hz, 1H), 6.82 (d, J = 8.7 Hz, 2H), 3.04 (s, 6H).

^{13}C NMR (151 MHz, $CDCl_3$) δ 192.79, 150.44, 143.62, 136.36, 131.05, 129.87, 124.01, 112.15, 40.34.

4-(Diphenylamino)biphenyl-2-carbaldehyde (3)[5]

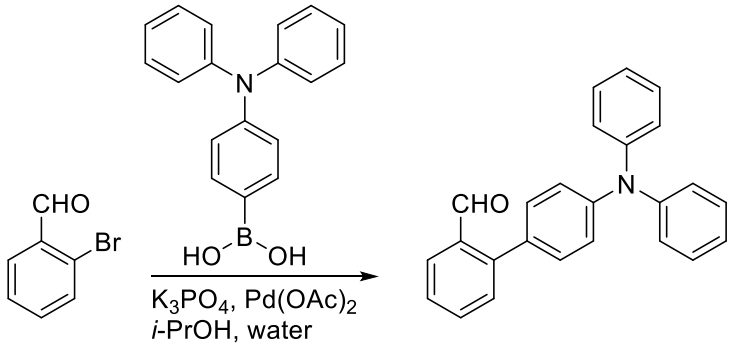

To a stirred solution of 2-bromobenzaldehyde (370 mg, 2 mmol) in isopropanol (10.8 mL), 4-(diphenylamino)phenylboronic acid (578 mg, 2 mmol) was added. This was followed by the addition of an aqueous solution of $K_3PO_4 \cdot 3H_2O$ (1.07 g, 4 mmol) in distilled water (5.2 mL). Finally, $Pd(OAc)_2$ (6.7 mg, 0.03 mmol) was added, and the reaction was placed in an oil bath preheated to 80 °C. The mixture was heated at this temperature for 20 min. After the specified time, the mixture was cooled to room temperature. Brine (15 mL) was added to the flask, and the aqueous phase was extracted with ethyl acetate (4 × 15 mL). The combined organic layers were dried over anhydrous Na_2SO_4.The solvent was removed under reduced pressure to yield the crude product. This residue was purified by flash column chromatography on silica gel, using a mixture of hexane:dichloromethane (*v*:*v*, 2:1) as the eluent. This yielded the final product as light-yellow crystals (630 mg, 90% yield).

Spectral data are identical to that previously published.[5]

^{1}H NMR (600 MHz, $CDCl_3$) δ 10.07 (t, J = 0.7 Hz, 1H), 8.02 – 7.99 (m, 1H), 7.62 (ddd, J = 7.6, 7.2, 1.4 Hz, 1H), 7.46 (dd, J = 7.7, 0.9 Hz, 2H), 7.29 (dd, J = 8.6, 7.3 Hz, 3H), 7.22 (d, J = 8.6 Hz, 2H), 7.18 – 7.12 (m, 6H), 7.07 (tt, J = 7.4, 1.2 Hz, 2H).

^{13}C NMR (151 MHz, $CDCl_3$) δ 192.66, 147.99, 147.33, 145.69, 133.66, 133.52, 130.91, 130.89, 130.61, 129.39, 127.57, 127.32, 124.84, 123.43, 122.48.

^{1}H and ^{13}C NMR spectra

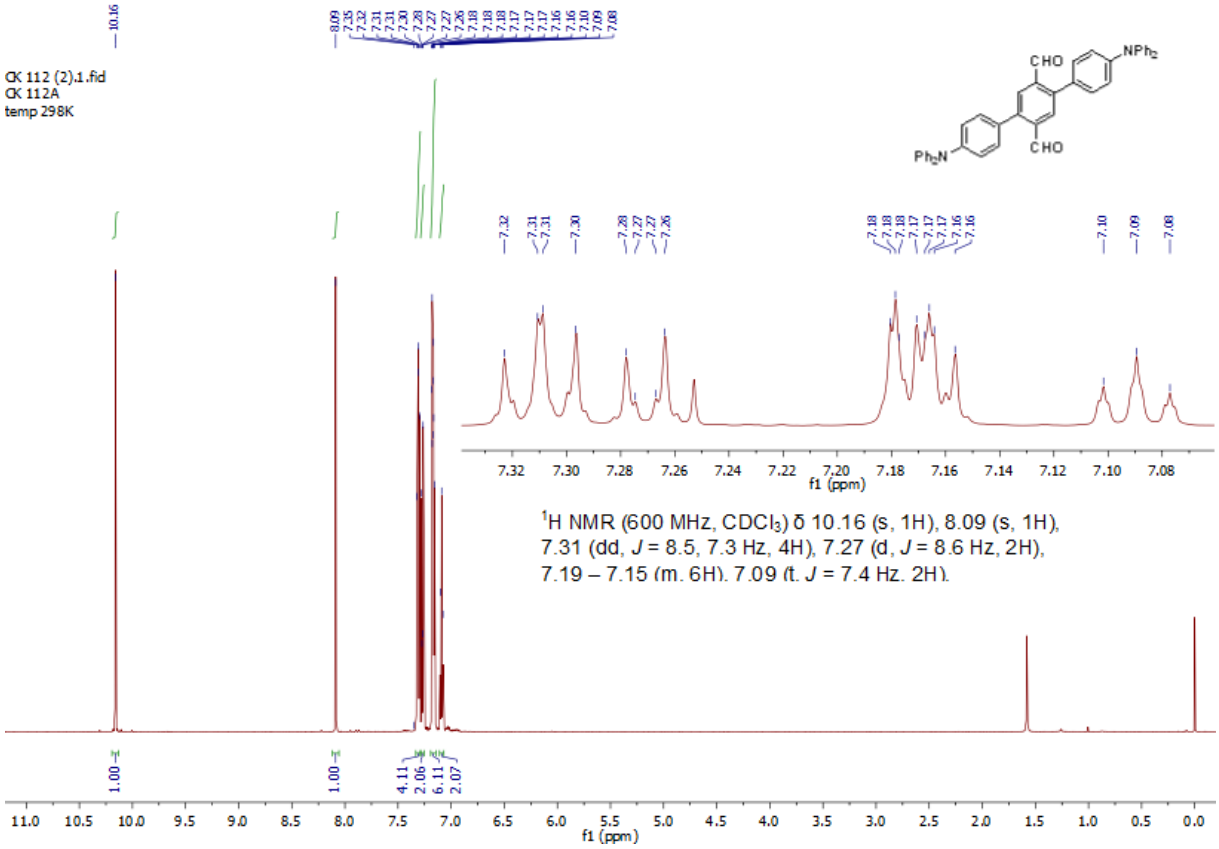

Figure S1. ^{1}H NMR spectrum of **1**.

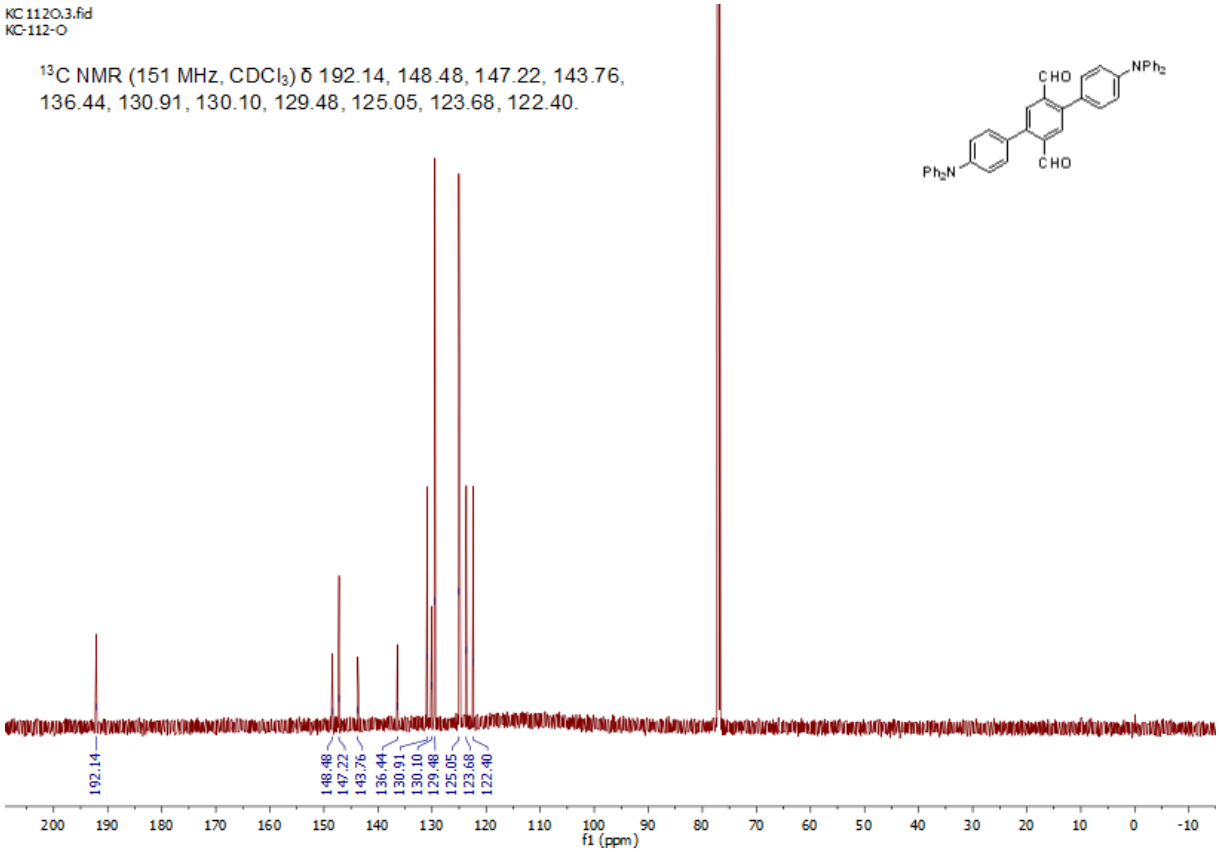

Figure S2. ^{13}C NMR spectrum of **1**.

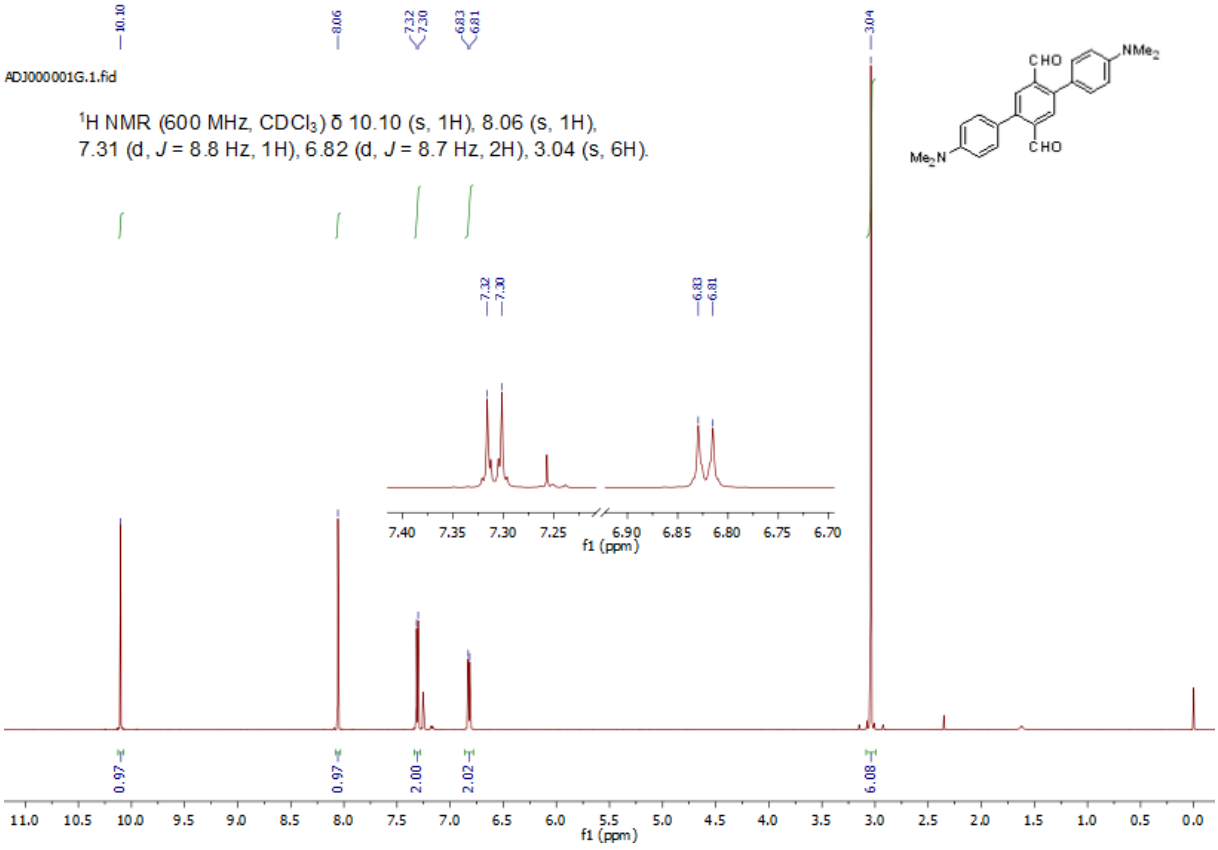

Figure S3. ^{1}H NMR spectrum of **2**.

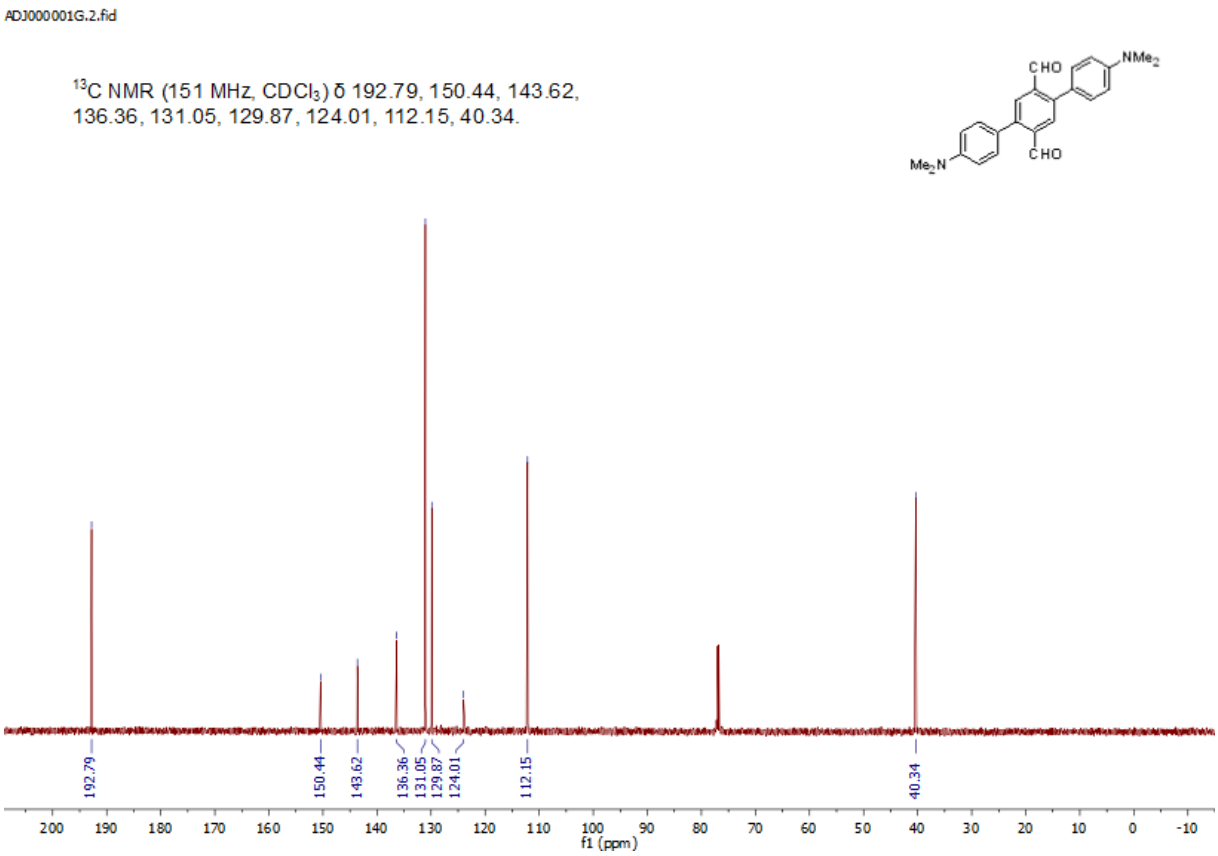

Figure S4. ^{13}C NMR spectrum of **2**.

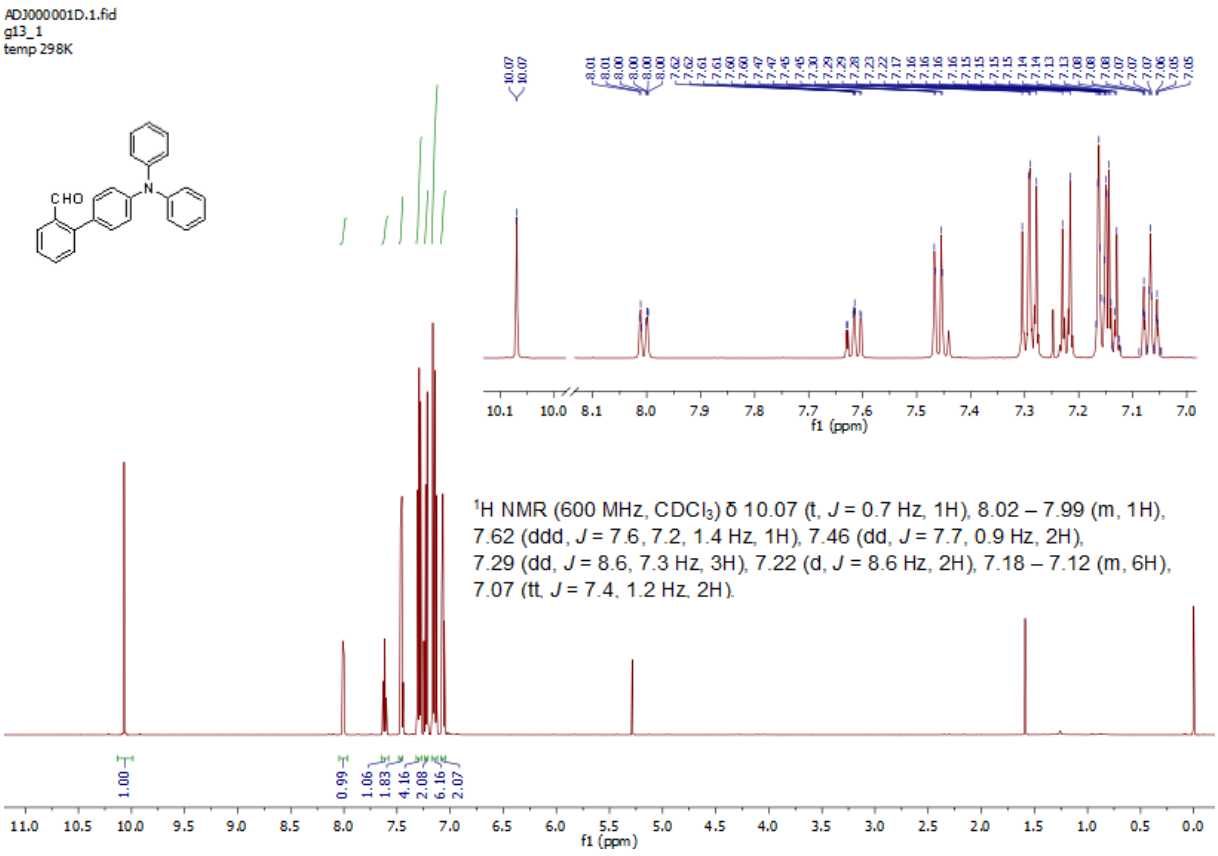

Figure S5. ^{1}H NMR spectrum of **3**.

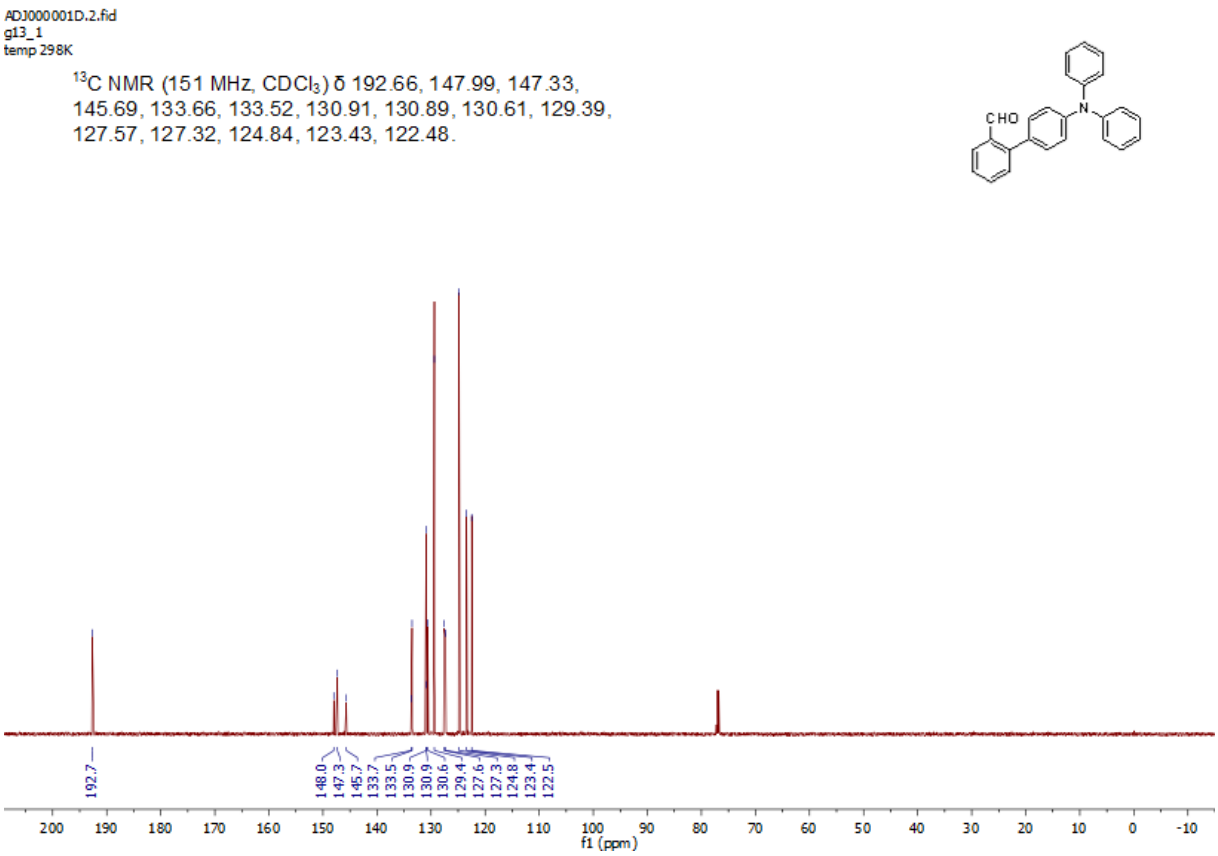

Figure S6. ^{13}C NMR spectrum of **3**.

UV-Vis and fluorescence measurements and spectra

Solution UV-Vis spectra were measured on a Hitachi U-1900 Spectrophotometer. The spectra were recorded in a quartz cuvette of 1 cm path length.

Fluorescence measurements in solution were acquired using a Hitachi F-7000 FL Spectrophotometer. The spectra were recorded in a quartz cuvette of 1 cm path length and with a 331 nm filter.

Fluorescence quantum yields in solution were determined with the Shimadzu UV-3600i Plus Spectrophotometer and FS5 spectrofluorometer from Edinburgh Instruments at 420 nm with coumarin 153 in acetonitrile (Φ_f = 56%) as a standard. The spectra were recorded in a quartz cuvette of 1 cm path length.

Excitation and emission spectra of solid-state samples and polymers were measured using the FS5 spectrofluorometer from Edinburgh Instruments.

Fluorescence quantum yields of solid-state samples and polymers were determined with the FLS 1000 spectrofluorometer from Edinburgh Instruments using an integrating sphere.

Preparation of PMMA samples:

1-**3**$_{PMMA}$ (0.02%): To a mixture of methyl methacrylate (MMA, 2 mL) and benzoyl peroxide (10 mg) in a 4 mL sealed vial, a luminophore (**1**-**3**, 0.4 mg) was added. The mixture was sonicated for 30 s and then heated at 80 °C for 30 minutes, then at 40 °C for 16 h and, finally, at 90 °C for 4 h. After that period, the samples were opened and kept at 60 °C for 2 days to dry. The vials were removed by breaking the glass, and the samples were analyzed.

1-**3**$_{PMMA}$ (0.002%): Luminophore (**1**-**3**, 0.4 mg) was dissolved in methyl methacrylate (MMA, 2 mL). Dissolved luminophore (0.2 mL) was added to a mixture of methyl methacrylate (MMA, 1.8 mL) and benzoyl peroxide (10 mg) in a 4 mL sealed vial. The mixture was sonicated for 30 s and then heated at 80 °C for 30 minutes, then at 40 °C for 16 h and, finally, at 90 °C for 4 h. After that period, the samples were opened and kept at 60 °C for 2 days to dry. The vials were removed by breaking the glass, and the samples were analyzed.

1-**3**$_{PMMA}$ (0.002%): Luminophore (**1**-**3**, 0.4 mg) was dissolved in methyl methacrylate (MMA, 2 mL). Dissolved luminophore (0.2 mL) was again dissolved in methyl methacrylate (MMA, 1.8 mL), and the obtained solution (0.2 mL) was added to a mixture of methyl methacrylate (MMA, 1.8 mL) and benzoyl peroxide (10 mg) in a 4 mL sealed vial. The mixture was sonicated for 30 s and then heated at 80 °C for 30 minutes, then at 40 °C for 16 h and, finally, at 90 °C for 4 h. After that period, the samples were opened and kept at 60 °C for 2 days to dry. The vials were removed by breaking the glass, and the samples were analyzed.

Preparation of mechanochemically treated samples:

The samples were prepared by placing compounds **1**-**3** (50 mg) in a 2 mL Eppendorf tube with 3 zirconium oxide balls (Ø = 5 mm) and milling in a horizontal mill Retsch MM400 for 15 min at 30 Hz.

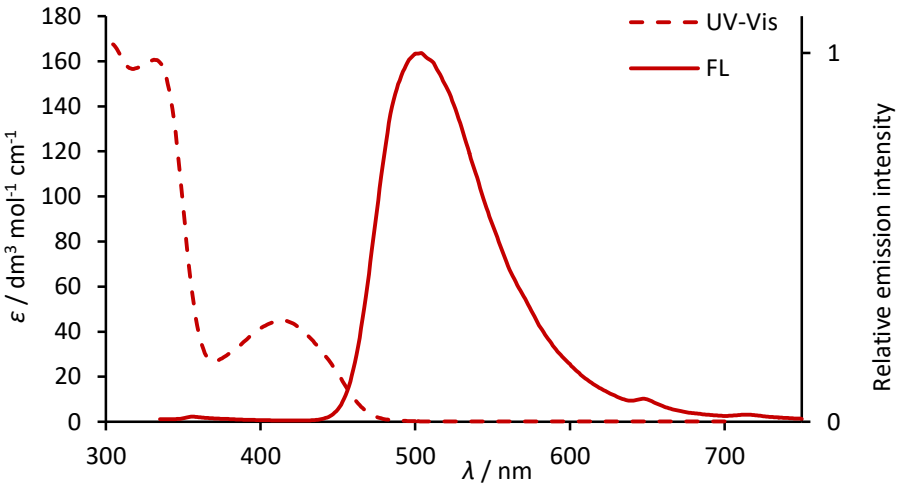

Figure S7. UV-Vis and fluorescence (irradiation at 320 nm) spectra of **1** in hexane.

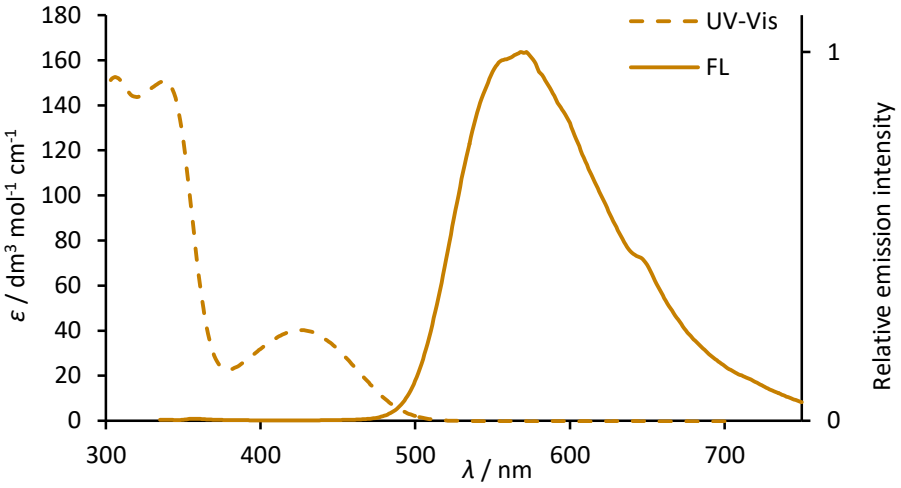

Figure S8. UV-Vis and fluorescence (irradiation at 320 nm) spectra of **1** in toluene.

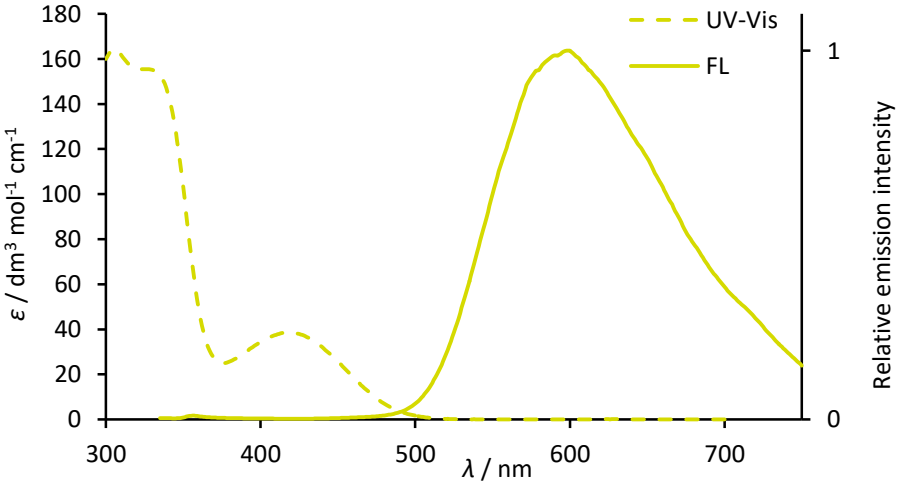

Figure S9. UV-Vis and fluorescence (irradiation at 320 nm) spectra of **1** in dioxane.

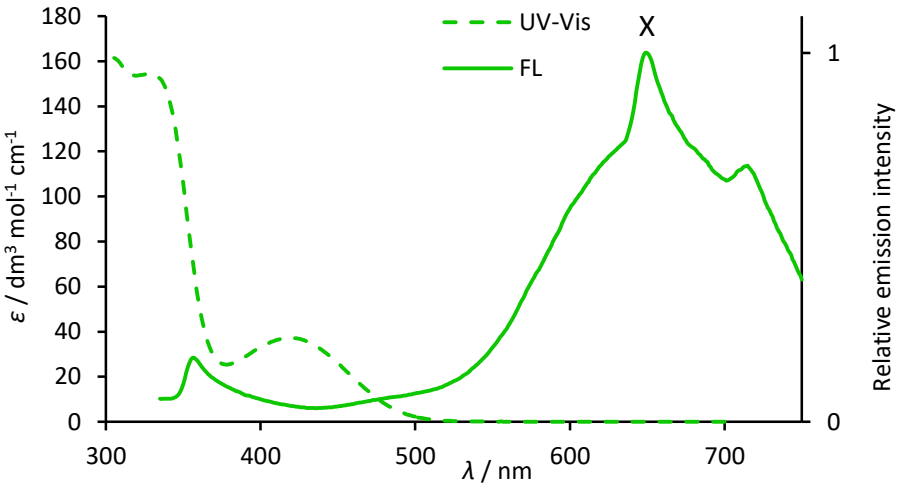

Figure S10. UV-Vis and fluorescence (irradiation at 320 nm) spectra of **1** in THF. X – 2nd order scattering.

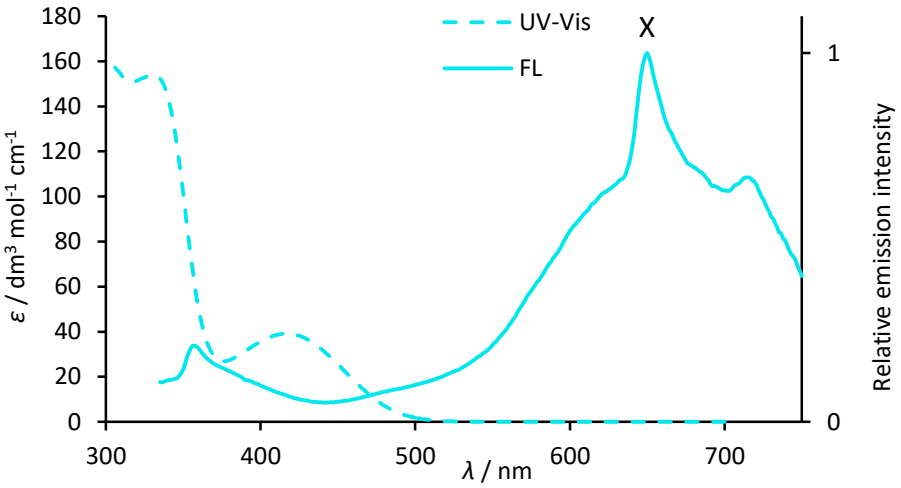

Figure S11. UV-Vis and fluorescence (irradiation at 320 nm) spectra of **1** in ethyl acetate. X – 2nd order scattering.

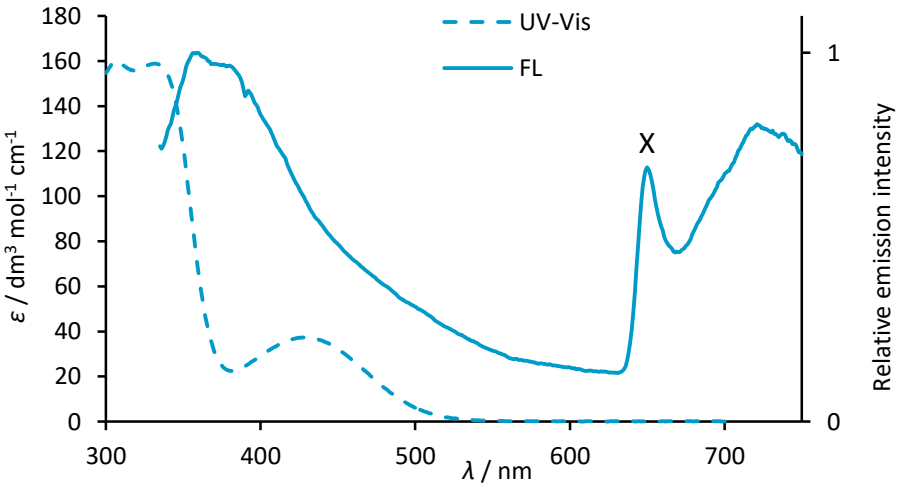

Figure S12. UV-Vis and fluorescence (irradiation at 320 nm) spectra of **1** in DCM. X – 2nd order scattering.

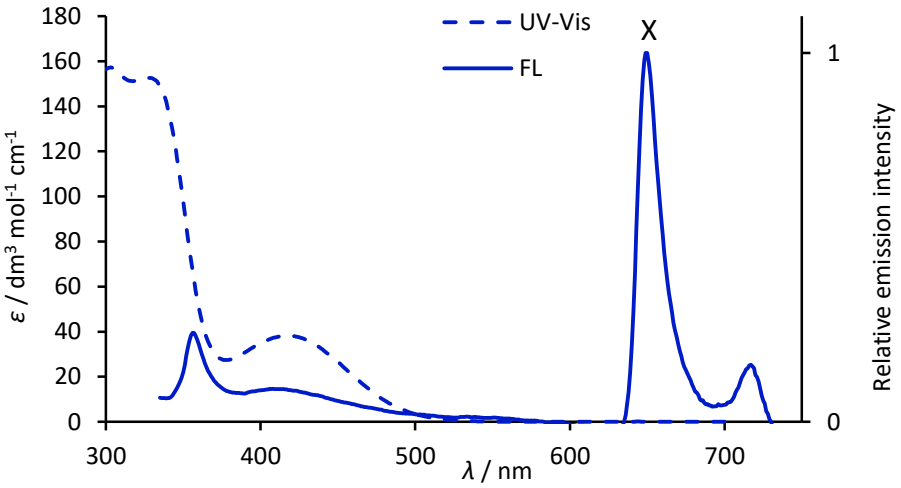

Figure S13. UV-Vis and fluorescence (irradiation at 320 nm) spectra of **1** in acetonitrile. X – 2nd order scattering.

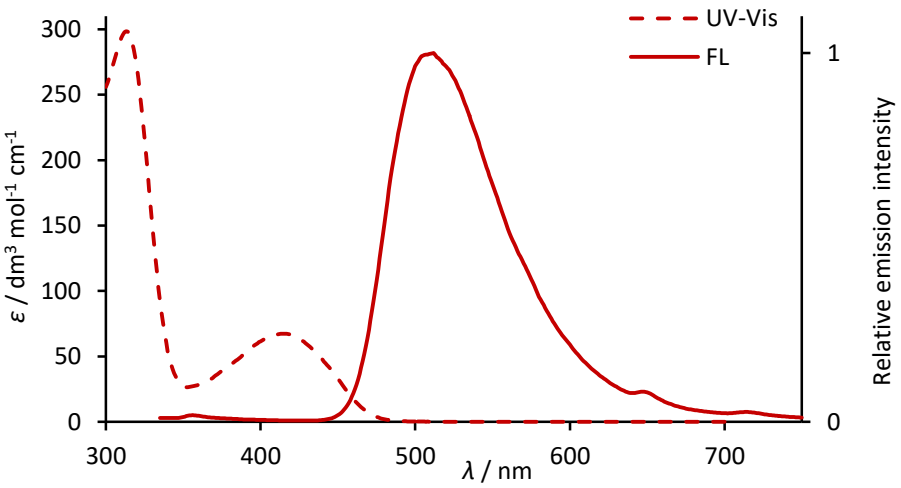

Figure S14. UV-Vis and fluorescence (irradiation at 320 nm) spectra of **2** in hexane.

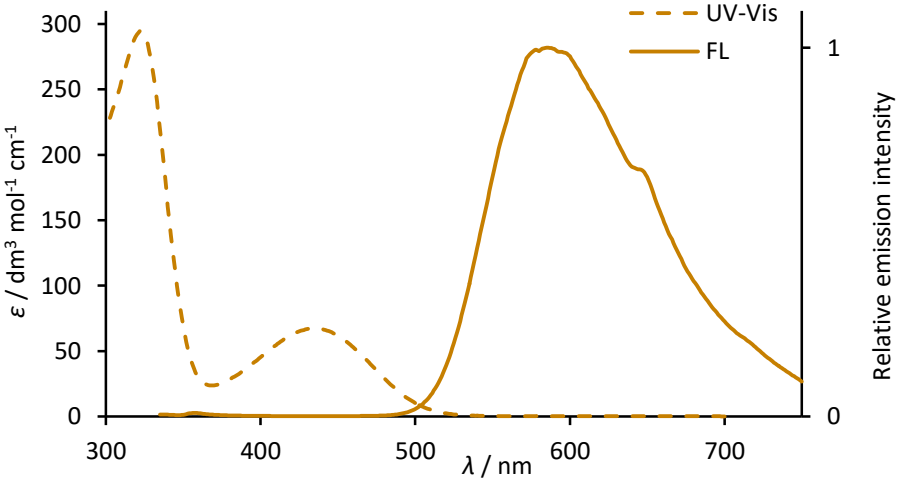

Figure S15. UV-Vis and fluorescence (irradiation at 320 nm) spectra of **2** in toluene.

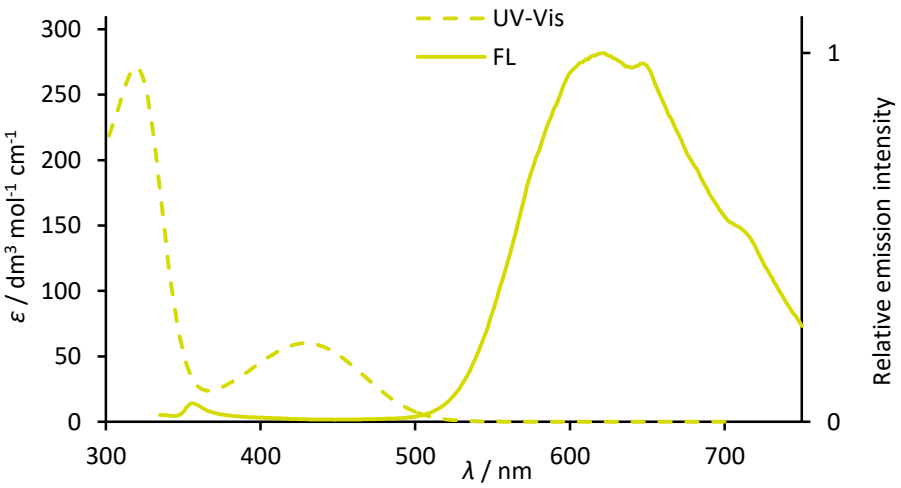

Figure S16. UV-Vis and fluorescence (irradiation at 320 nm) spectra of **2** in dioxane.

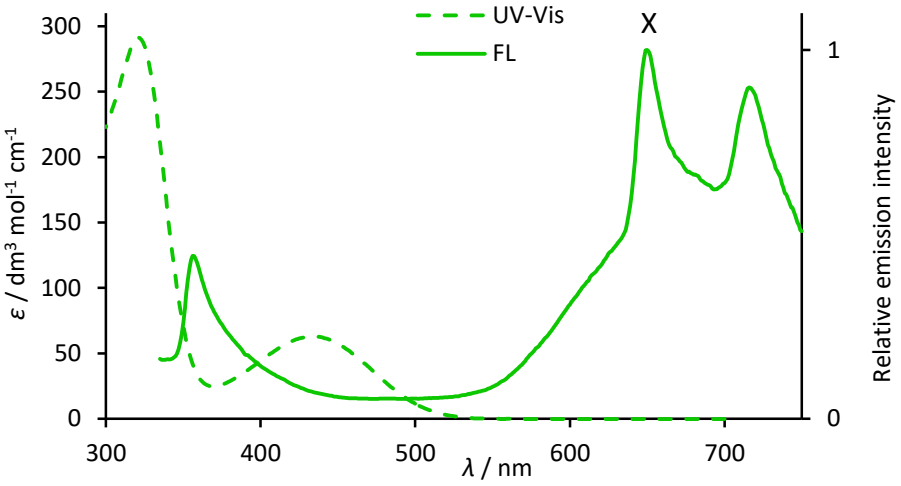

Figure S17. UV-Vis and fluorescence (irradiation at 320 nm) spectra of **2** in THF. X – 2nd order scattering.

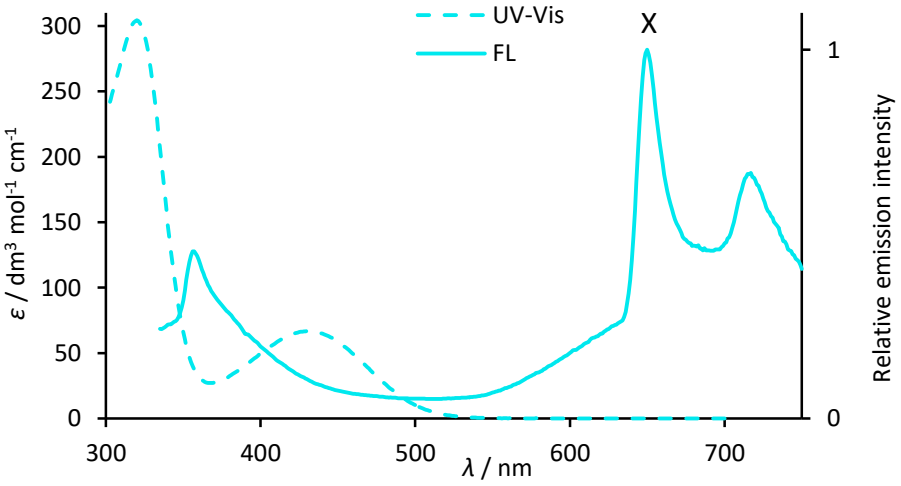

Figure S18. UV-Vis and fluorescence (irradiation at 320 nm) spectra of **2** in ethyl acetate. X – 2nd order scattering.

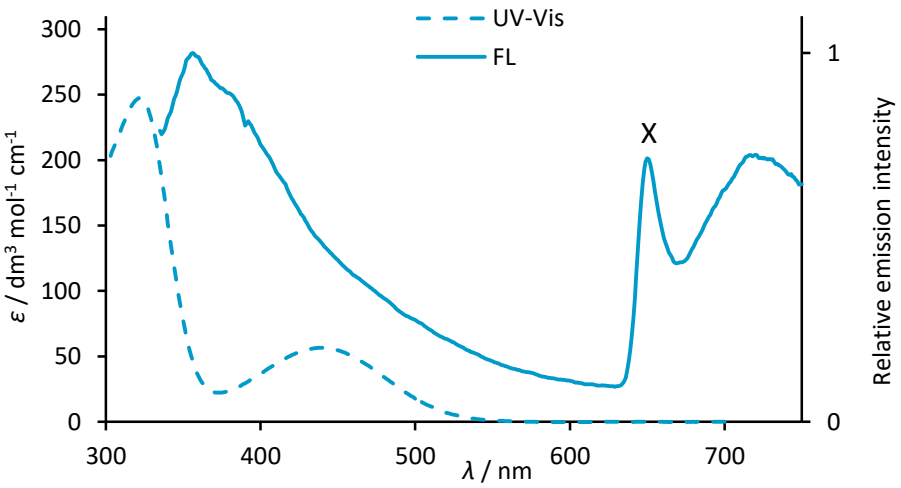

Figure S19. UV-Vis and fluorescence (irradiation at 320 nm) spectra of **2** in DCM. X – 2nd order scattering.

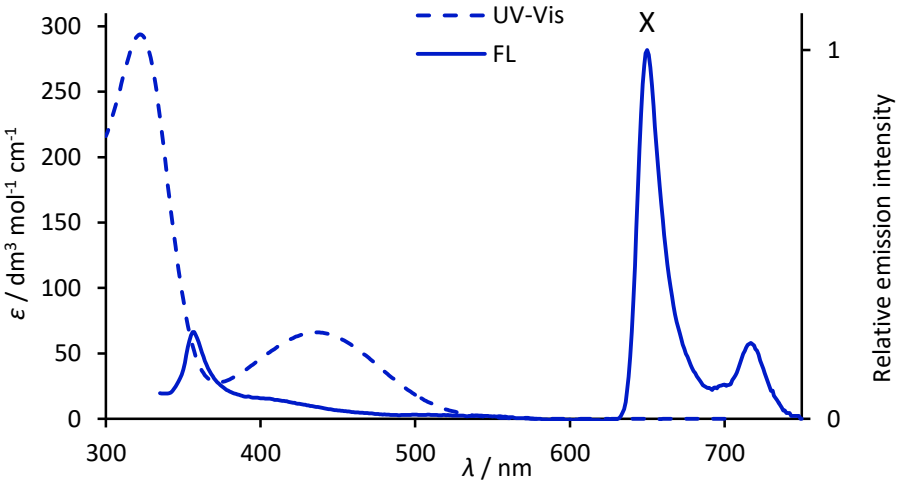

Figure S20. UV-Vis and fluorescence (irradiation at 320 nm) spectra of **2** in acetonitrile. X – 2nd order scattering.

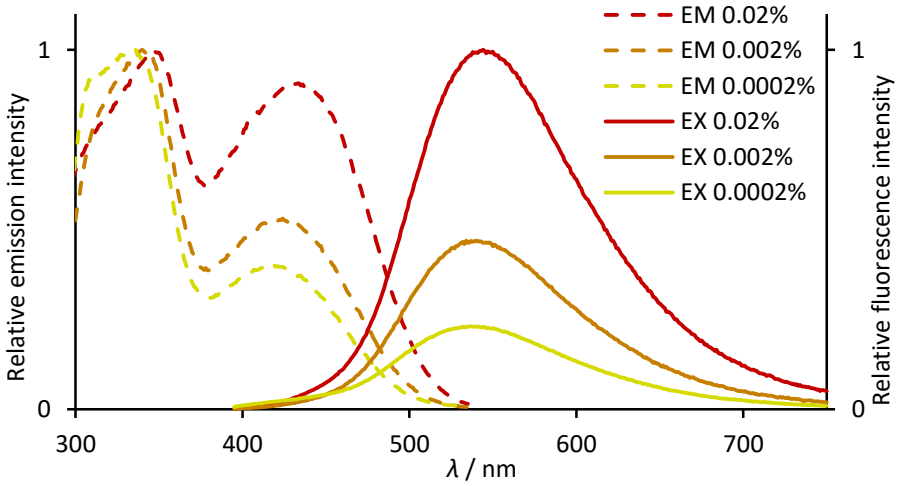

Figure S21. Emission (detection at 550 nm) and fluorescence (irradiation at 340 nm) spectra of **1** in PMMA matrix.

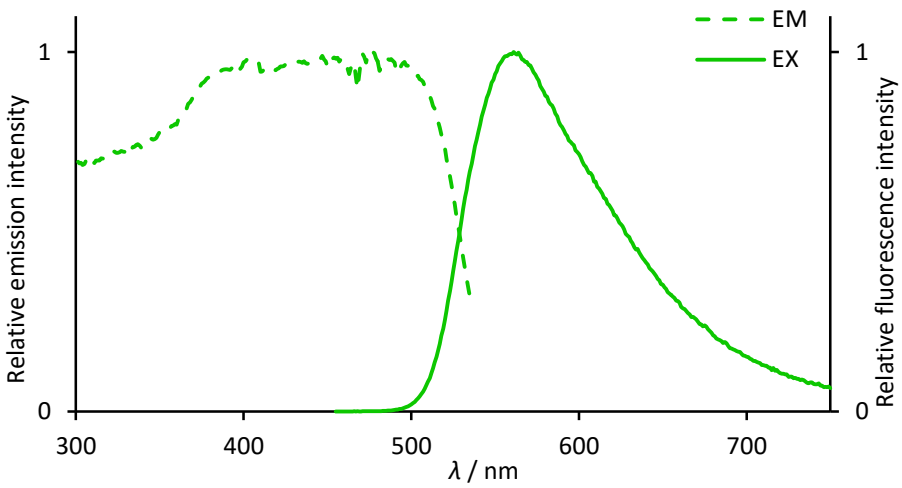

Figure S22. Emission (detection at 570 nm) and fluorescence (irradiation at 400 nm) spectra of **1** in solid state.

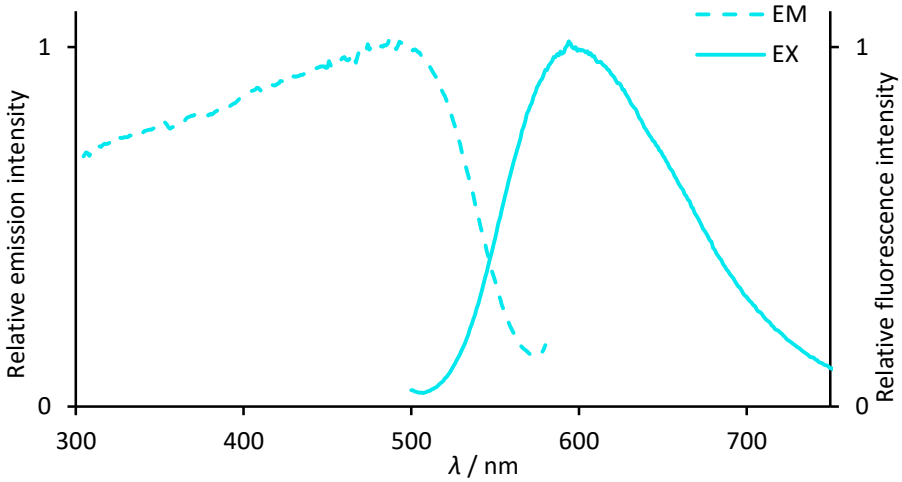

Figure S23. Emission (detection at 597 nm) and fluorescence (irradiation at 485 nm) spectra of **1** in solid state after milling.

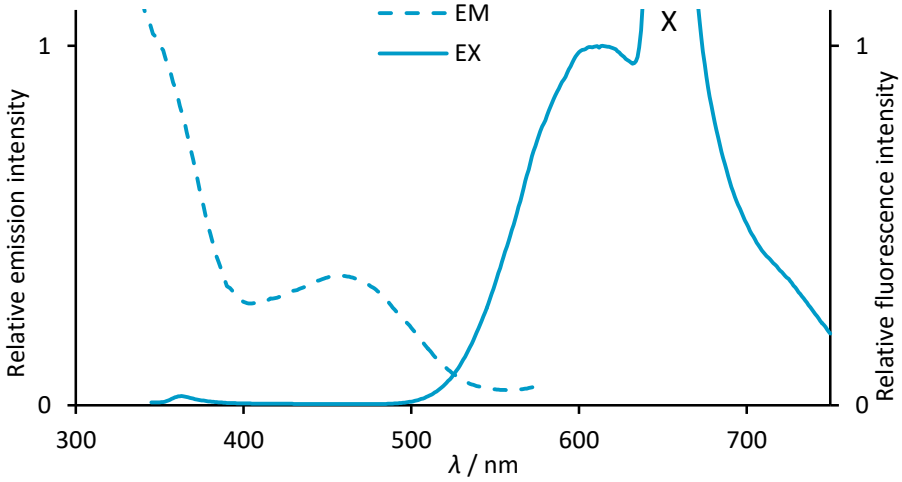

Figure S24. Emission (detection at 593 nm) and fluorescence (irradiation at 320 nm) spectra of **1** in water. X – 2nd order scattering.

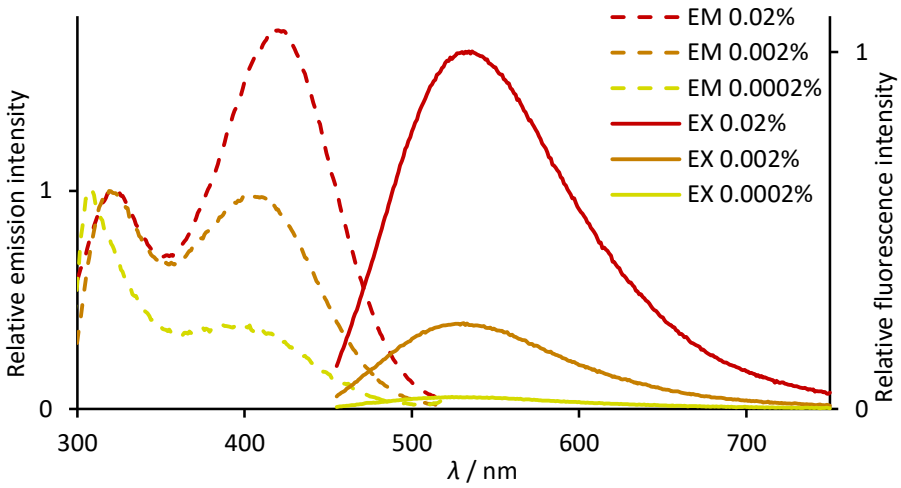

Figure S25. Emission (detection at 535 nm) and fluorescence (irradiation at 415 nm) spectra of **2** in PMMA matrix.

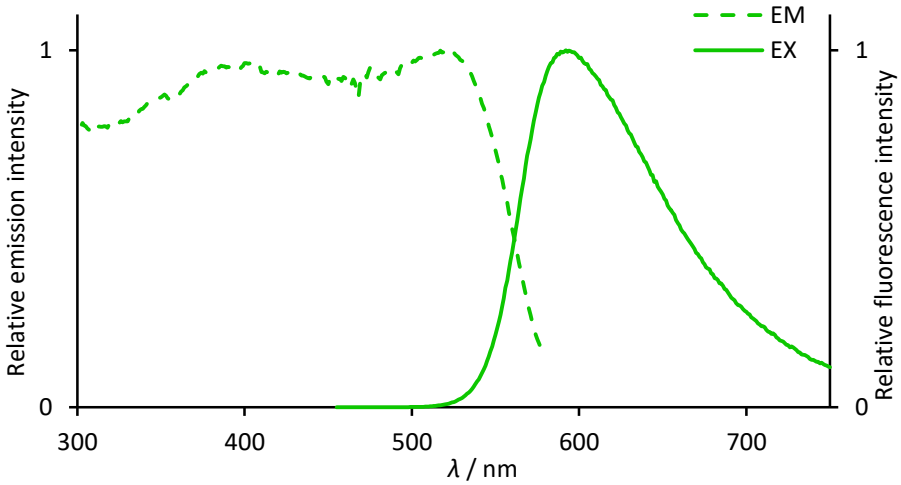

Figure S26. Emission (detection at 595 nm) and fluorescence (irradiation at 405 nm) spectra of **2** in solid state.

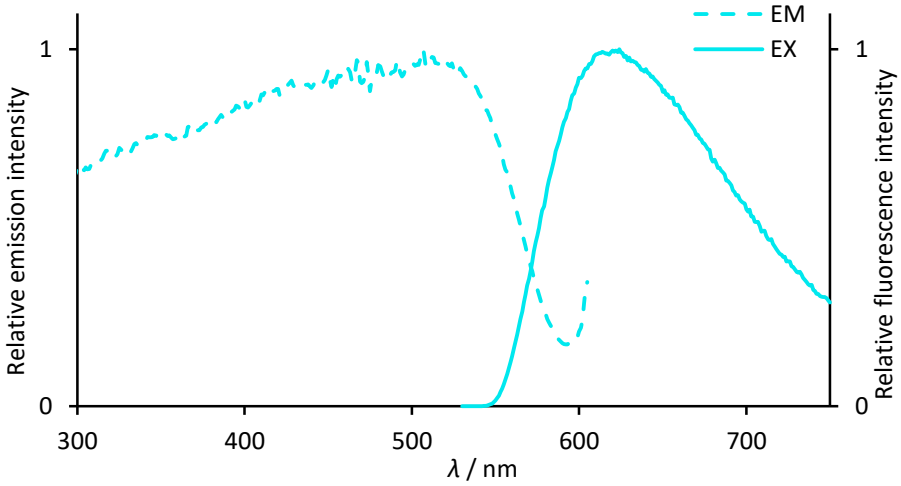

Figure S27. Emission (detection at 620 nm) and fluorescence (irradiation at 515 nm) spectra of **2** in solid state after milling.

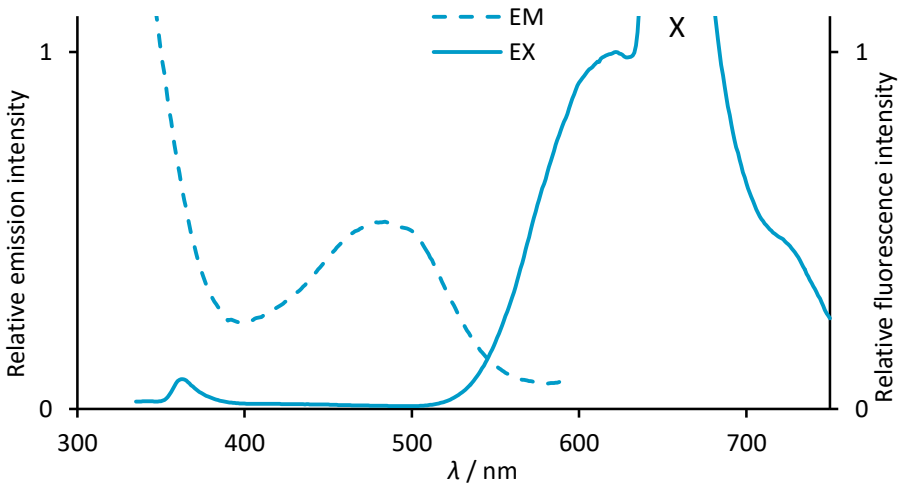

Figure S28. Emission (detection at 605 nm) and fluorescence (irradiation at 325 nm) spectra of **2** in water. X – 2nd order scattering.

Calculations

Conformational Analysis

Conformational searches for molecules **1** and **2** were performed using molecular mechanics (MM) as implemented in the Scigress software package.[6] The resulting conformers were then optimized using a Density Functional Theory (DFT) approach with the B3LYP hybrid functional and the 6-311G(d,p) basis set.[7] All DFT calculations were performed using the Gaussian 16 software package.[8]

For molecule **1**, the energy differences among the ten lowest-energy conformers were found to be negligible. To confirm this, recalculations were performed using the B2PLYP double-hybrid functional, which incorporates an MP2-like correlation.[9] This method yielded even smaller energy differences. As these calculated energy differences are negligible and within the margin of error for the methods, all conformers were considered to contribute equally to the overall conformational distribution.

Calculations for compound **2** were conducted similarly, yielding two conformers of nearly equal energy. The conformers' energies were not recalculated with the B2PLYP functional, as this was not expected to significantly alter their relative stability.

For molecule **3**, the focus was on comparing its orbital shapes with those calculated for molecules **1** and **2**. Therefore, no conformational search was conducted. Instead, a single conformer was generated by manually modifying the lowest-energy conformer of molecule **1**, and its geometry was optimized using the same method.

Calculation of Spectroscopic Properties

To select the most appropriate functional for calculating spectroscopic properties, several functionals (CAM-B3LYP,[10] BH&HLYP,[8] M06-HF,[11] and M06-2X[12]) were benchmarked using a representative conformer of compound **1**. The CAM-B3LYP, BH&HLYP, and M06-2X functionals produced analogous results that aligned with experimental data, whereas the M06-HF functional failed to reproduce the experimental spectrum. Consequently, the CAM-B3LYP functional was chosen for all subsequent spectroscopic property calculations.

Natural transition orbitals (NTOs)[13] were calculated using the implementation within Gaussian 16. Orbital and electron difference density visualizations were generated with the GaussView program.[14]

Intermolecular Stacking Analysis

To investigate the potential for intermolecular stacking of luminophore **1**, a series of calculations were performed on trimeric systems. To remain consistent with experimental data, this study was restricted to systems of three molecules arranged in stacks. The initial geometries for these trimers were derived from available X-ray crystal structures of the

polymorphs of **1**. The systems are therefore denoted as **1α**, **1β**, **1γ**, and **1δ**, corresponding to the known crystalline phases.

Each trimolecular system was fully optimized at the DFT level using various combinations of functionals (B3LYP, APF, APFD, M06L) and basis sets.[7,11,15] The GD3BJ empirical dispersion correction was included to properly account for non-covalent interactions, particularly when using the B3LYP functional.[16]

Four of the tested methods provided consistent results, identifying the **1β** trimer as the most energetically favorable arrangement (see Tables S4-S8). The preference for the **1β** structure is attributed to the maximization of π···π interactions between the terminal phenyl rings of the two outer molecules and the central unit. This arrangement involves a slight deviation from a perfectly parallel orientation, allowing the remaining aromatic rings to adopt a conformation that facilitates additional CH···π interactions. A comparison between the trimolecular fragments found in the crystal structures and those optimized at the DFT level is provided in Figures S43-S46.

Table S1. Calculated relative energies of individual conformers of **1** (ΔE, $\Delta\Delta G$ in kcal mol^{-1}), their percentage populations (%E, %ΔG), and their symmetries. In the case of enantiomers, the total percentage of populations is provided.

	Method						
	B3LYP/6-311g(d,p)[a]				B2PLYP/6-311g(d,p)[b]		
Conformer no	ΔE	$\Delta\Delta G$	%E	%ΔG	ΔE	%E	Symmetry
1	0.09	0.00	11.72	12.11	0.00	19.02	C_i
2[c]	0.00	0.02	13.55	11.76	0.00	19.09	C_2
3[c]	0.00	0.02	13.55	11.76			C_2
4[c]	0.24	0.07	9.10	10.78	0.08	16.78	C_1
5[c]	0.24	0.07	9.10	10.76			C_1
6[c]	0.17	0.13	10.25	9.65	0.08	16.78	C_1
7[c]	0.17	0.13	10.25	9.65			C_1
8[c]	0.33	0.24	7.74	8.12	0.18	14.19	C_2
9[c]	0.33	0.24	7.74	8.12			C_2
10	0.39	0.30	7.00	7.29	0.17	14.26	C_i

[a] – fully optimized geometry; [b] – single point energy for geometry optimized at the B3LYP/6-311G(d,p) level; [c] – enantiomers

Table S2. A comparison of the results of the TD-DFT calculation (energy of transition as wavelength λ in nm, oscillator strength f) using CAM-B3LYP, BH&HLYP, M06-HF, and M06-2X functionals for conformer no. 1 of compound **1** for 20 transitions with a 6-311g(d,p) basis set.

	Functional							
	CAM-B3LYP		BH&HLyp		M06-HF		M06-2X	
Transition no.	λ	f	λ	f	λ	f	λ	f
1	362.23	0.3006	357.42	0.3414	403.93	0	372.43	0.1993
2	340.93	0	330.71	0	403.54	0.0048	357.65	0
3	325.10	0.2045	312.51	0	294.15	1.3819	337.84	0.2814
4	319.22	0	310.98	0.1224	272.36	0	327.65	0
5	294.66	1.0034	288.55	1.0676	267.43	0.3062	297.78	1.0534
6	286.54	0	277.72	0	262.14	0	287.64	0
7	285.35	0.0933	276.10	0.0742	259.68	0.1498	285.44	0.0873
8	279.71	0	273.13	0	254.52	0	282.15	0
9	270.90	0	262.76	0.1285	254.34	0.4329	272.49	0
10	270.79	0.4382	262.31	0	236.51	0.2947	272.38	0.4385
11	265.27	0.1319	262.20	0.4171	235.48	0	264.35	0.1009
12	253.27	0.0487	249.80	0.2213	232.75	0.0531	251.19	0.0218
13	251.93	0	243.66	0	228.18	0	250.58	0
14	249.73	0.2281	242.98	0.1193	227.78	0.0803	247.71	0.1712
15	246.95	0.0890	238.55	0.0928	227.18	0	245.44	0
16	246.78	0	238.30	0	215.10	0.4508	245.43	0.1527
17	233.44	0.2095	230.57	0.1429	211.72	0.0977	236.55	0.1805
18	229.09	0	229.81	0	200.58	0	235.59	0
19	228.55	0	228.80	0	198.32	0	229.08	0
20	228.35	0.0265	228.30	0.0195	198.21	0.2841	228.82	0.0251

Table S3. Calculated relative energies of individual conformers of 2 (ΔE, $\Delta\Delta G$ in kcal mol^{-1}), their percentage populations (%E, %ΔG), and their approximate symmetries.

	B3LYP/6-311g(d,p)				
Conformer no.	ΔE	$\Delta\Delta G$	%E	%ΔG	approximate symmetry
1	0.00	0.00	52.90	55.1	C_2
2	0.07	0.12	47.18	44.9	C_i

Table S4. Total energies (*E*, in Hartree), relative energies (Δ*E*, ΔΔ*G* in kcal mol^{-1}), and percentage populations (%*E*, %Δ*G*) of trimolecular systems **1α**, **1β**, **1γ**, and **1δ** composed of three molecules of **1** and calculated at the B3LYP/6-31G(d) level of theory The initial geometries were derived from available X-ray data.

System	*E*	Δ*E*	%*E*	ΔΔ*G*	%Δ*G*
1α	-5867.71078	1.36	5.85	0.43	20.31
1β	-5867.71211	0.52	23.80	0	41.93
1γ	-5867.71084	1.32	6.24	2.13	
1δ	-5867.71294	0	57.74	2.94	

Table S5. Total energies (*E*, in Hartree), relative energies (Δ*E*, ΔΔ*G* in kcal mol^{-1}), and percentage populations (%*E*, %Δ*G*) of trimolecular systems **1α**, **1β**, **1γ**, and **1δ** composed of three molecules of **1** and calculated at the B3LYP-GD3BJ/6-31G(d) level of theory The initial geometries were derived from available X-ray data.

System	*E*	Δ*E*	%*E*	ΔΔ*G*	%Δ*G*
1α	-5868.45488	11.97		7.26	
1β	-5868.47395	0	100	0	100
1γ	-5868.46233	7.29		6.47	
1δ	-5868.46206	7.46		6.33	

Table S6. Total energies (*E*, in Hartree), relative energies (Δ*E*, ΔΔ*G* in kcal mol^{-1}), and percentage populations (%*E*, %Δ*G*) of trimolecular systems **1α**, **1β**, **1γ**, and **1δ** composed of three molecules of **1** and calculated at the APF/6-31G(d) level of theory The initial geometries were derived from available X-ray data.

System	*E*	Δ*E*	%*E*	ΔΔ*G*	%Δ*G*
1α	-5862.78339	0.44	19.43	3.05	
1β	-5862.78311	0.61	14.39	2.49	
1γ	-5862.78269	0.87	9.28	3.36	
1δ	-5862.78409	0	40.56	0	94.42

Table S7. Total energies (*E*, in Hartree), relative energies (Δ*E*, ΔΔ*G* in kcal mol^{-1}), and percentage populations (%*E*, %Δ*G*) of trimolecular systems **1α**, **1β**, **1γ**, and **1δ** composed of three molecules of **1** and calculated at the APFD/6-31G(d) level of theory The initial geometries were derived from available X-ray data.

System	*E*	Δ*E*	%*E*	ΔΔ*G*	%Δ*G*
1α	-5863.14274	12.29		7.38	
1β	-5863.16233	0	100	0	100
1γ	-5863.1522	6.36		6.20	
1δ	-5863.15154	6.77		5.27	

Table S8. Total energies (*E*, in Hartree), relative energies (Δ*E*, ΔΔ*G* in kcal mol^{-1}), and percentage populations (%*E*, %Δ*G*) of trimolecular systems **1α**, **1β**, **1γ**, and **1δ** composed of three molecules of **1** and calculated at the M06L/6-31G(d) level of theory The initial geometries were derived from available X-ray data.

System	*E*	Δ*E*	%*E*	ΔΔ*G*	%Δ*G*
1α	-5867.08152	8.31		5.62	
1β	-5867.09477	0	100	0	100
1γ	-5867.08369	6.96		4.87	
1δ	-5867.08323	7.24		3.99	

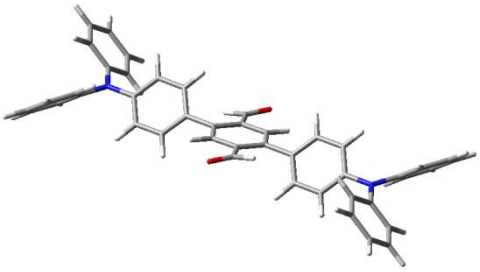

conf 1

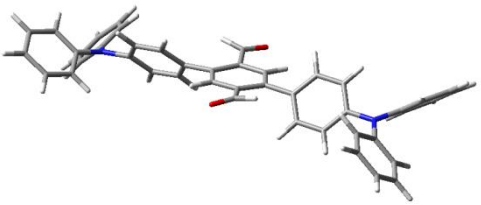

conf 2

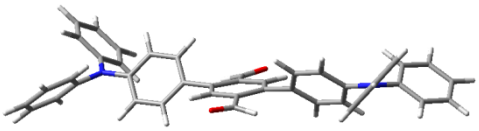

conf 3

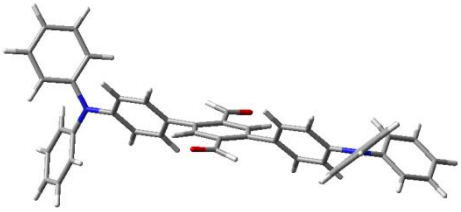

conf 4

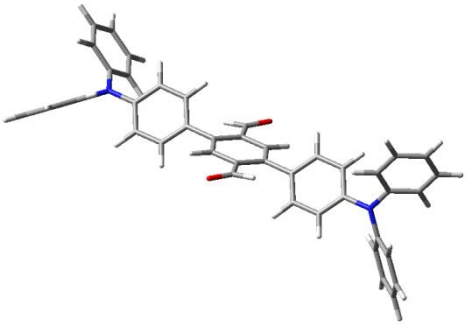

conf 5

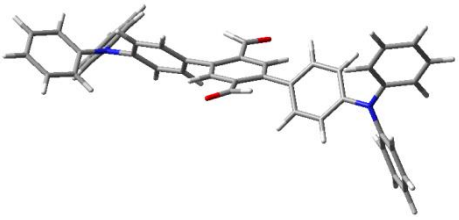

conf 6

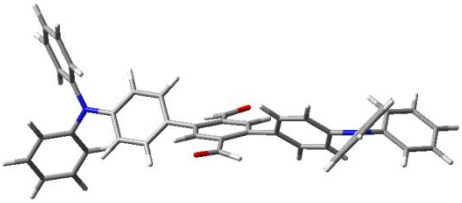

conf 7

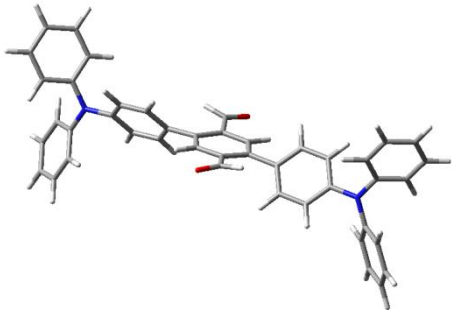

conf 8

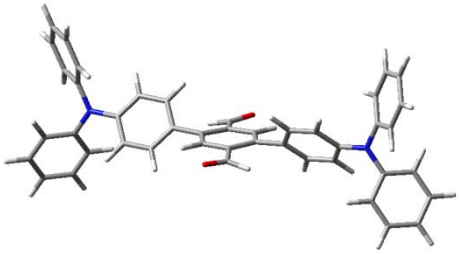

conf 9

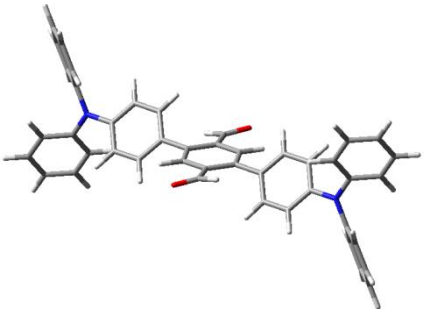

conf 10

Figure S29. Optimized conformers of **1** (B3LYP/6-311g(d,p)).

CAM-B3LYP

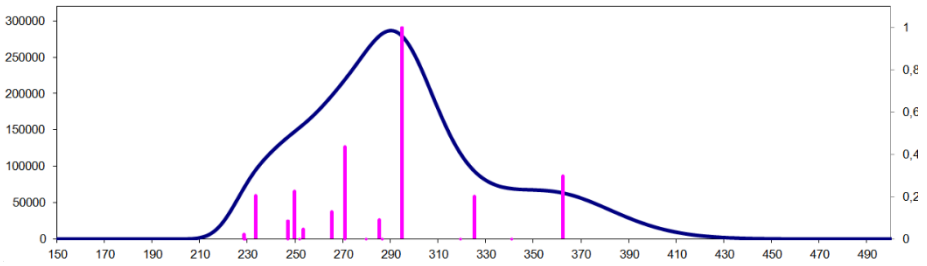

H&HLYP

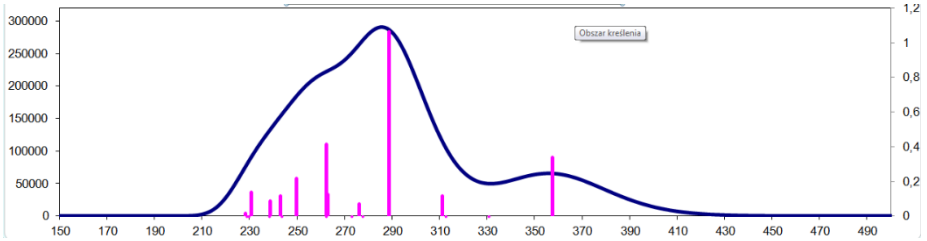

M06-HF

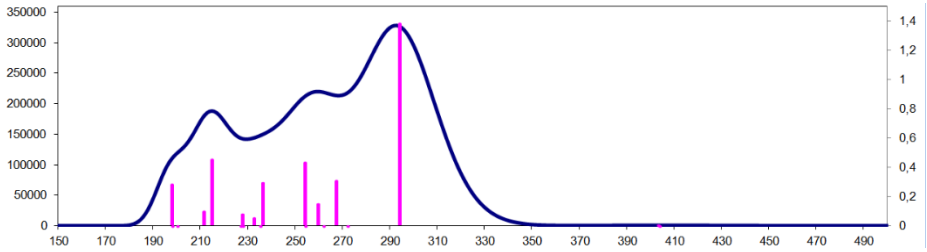

M06-2X

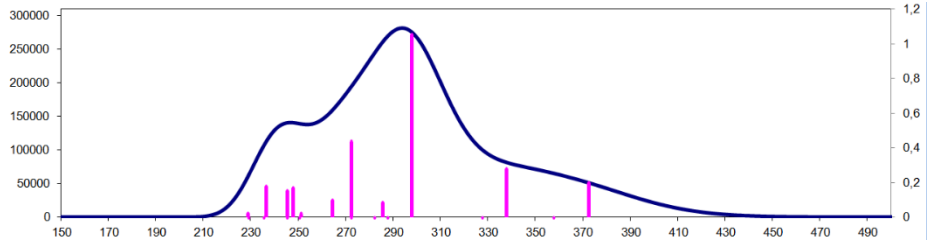

Figure S30 UV-Vis spectra of conformer no. 1 of **1** calculated with the use of different functionals and 6-311g(d,p) basis set. Calculations were performed for 20 excited states (left axis arbitrary units, right axis oscillator strength).

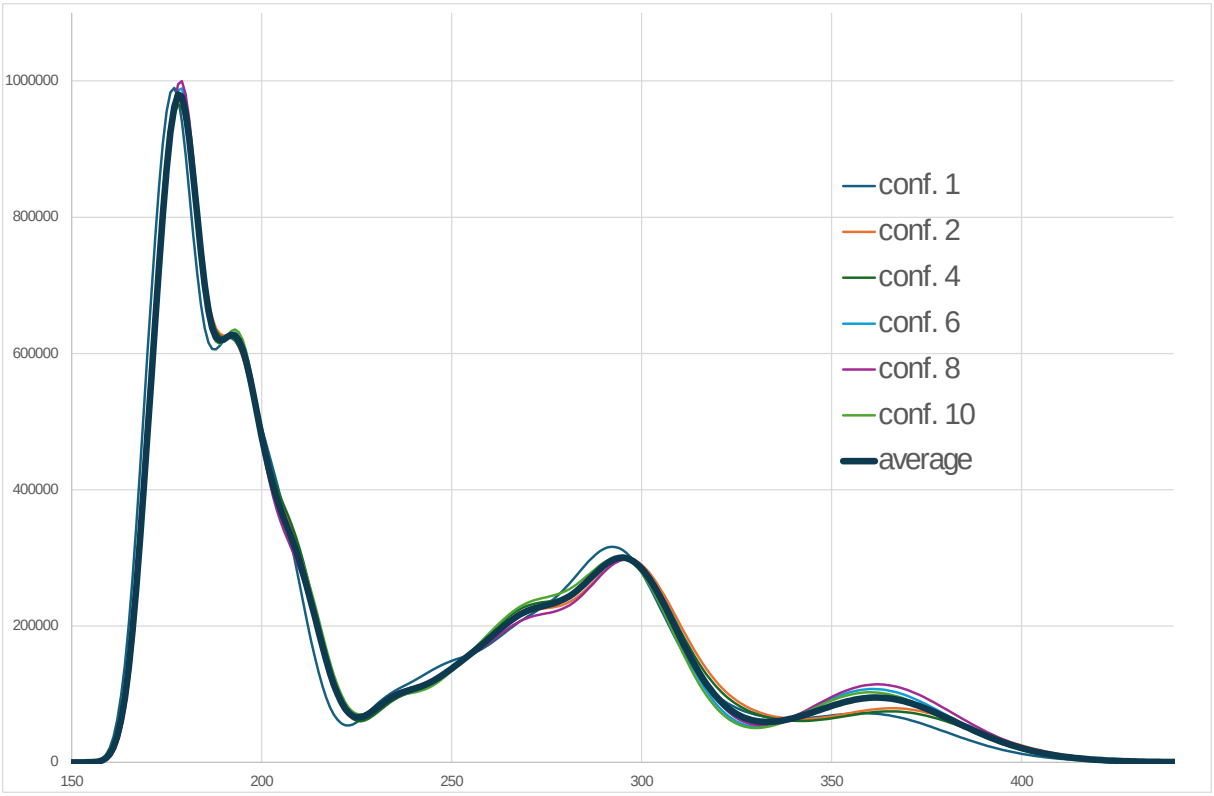

Figure S31. UV-Vis spectra calculated for individual conformers of **1**, and the ΔΔ*G*-based and Boltzmann-averaged UV-Vis spectrum calculated for **1**. The UV-Vis spectra of conformers no. 3, 5, 7, and 9 are not shown as they are identical with the spectra of their enantiomers no. 2, 4, 6, and 10, respectively.

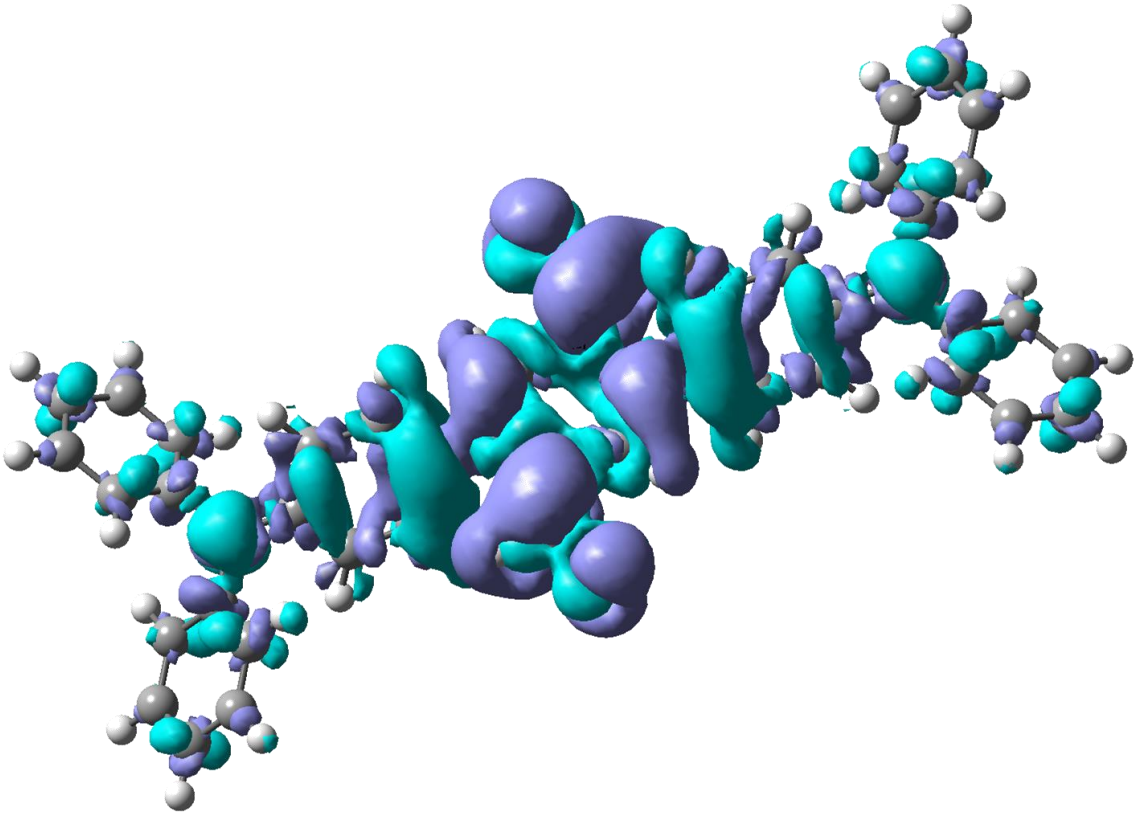

Figure S32. Electron difference density between the first excited state (blue) and the ground state (greenish) in conformer no. 1 of the compound **1**.

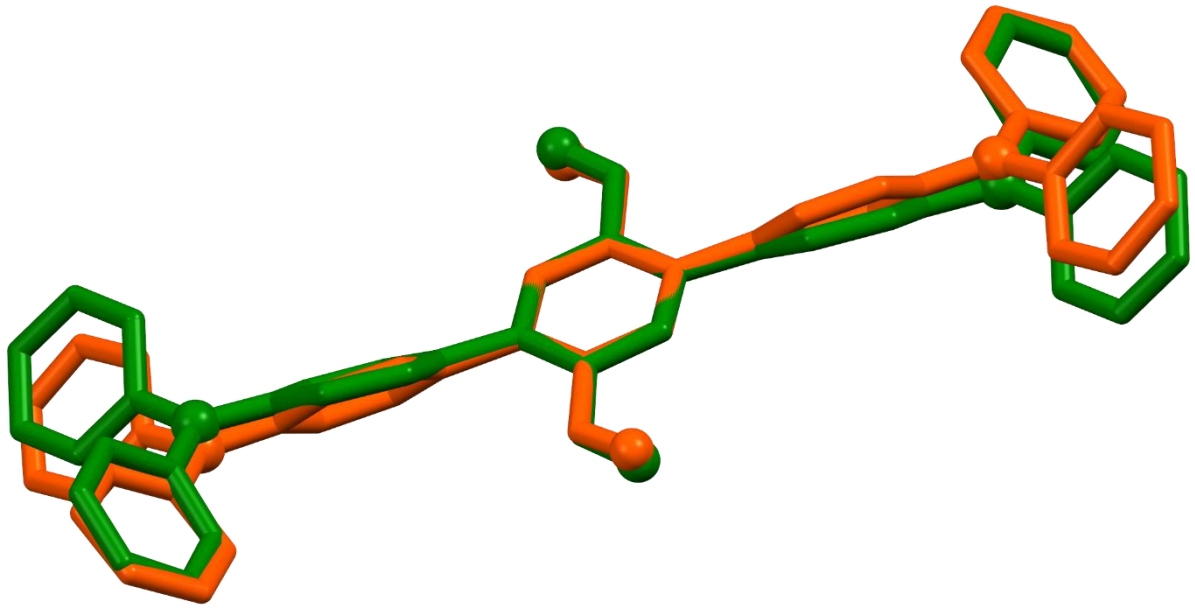

Figure S33. Overlap of structures of the excited and the ground states of compound **1**, conf no. 1.

a)

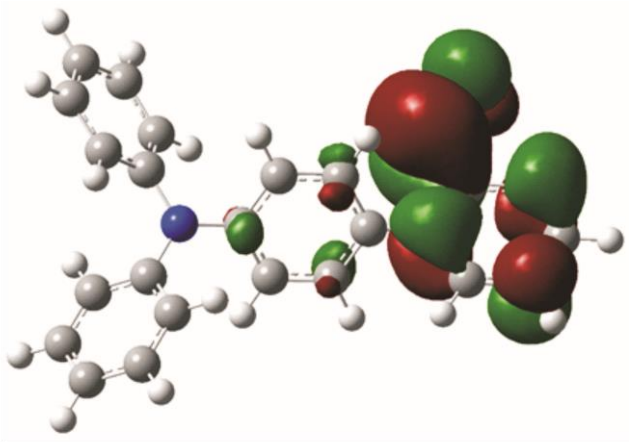

b)

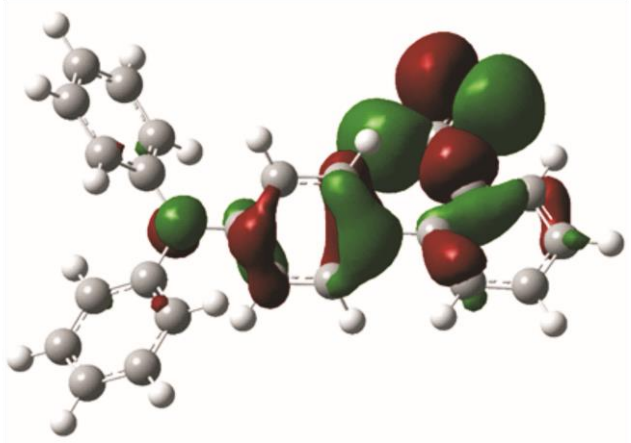

Figure S34. Natural transition orbitals on conformer no. 1 of the compound **3**. a) LUTO – lowest unoccupied transition orbital b) HOTO – highest occupied transition orbital.

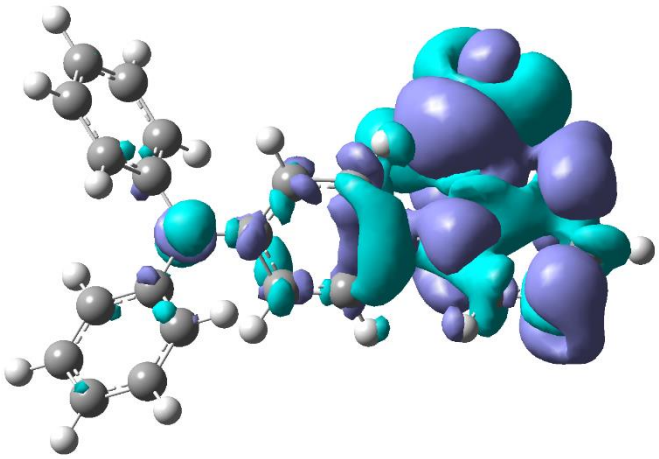

Figure S35. Electron difference density between the first excited state (blue) and the ground state (greenish) in conformer no. 1 of the compound **3**.

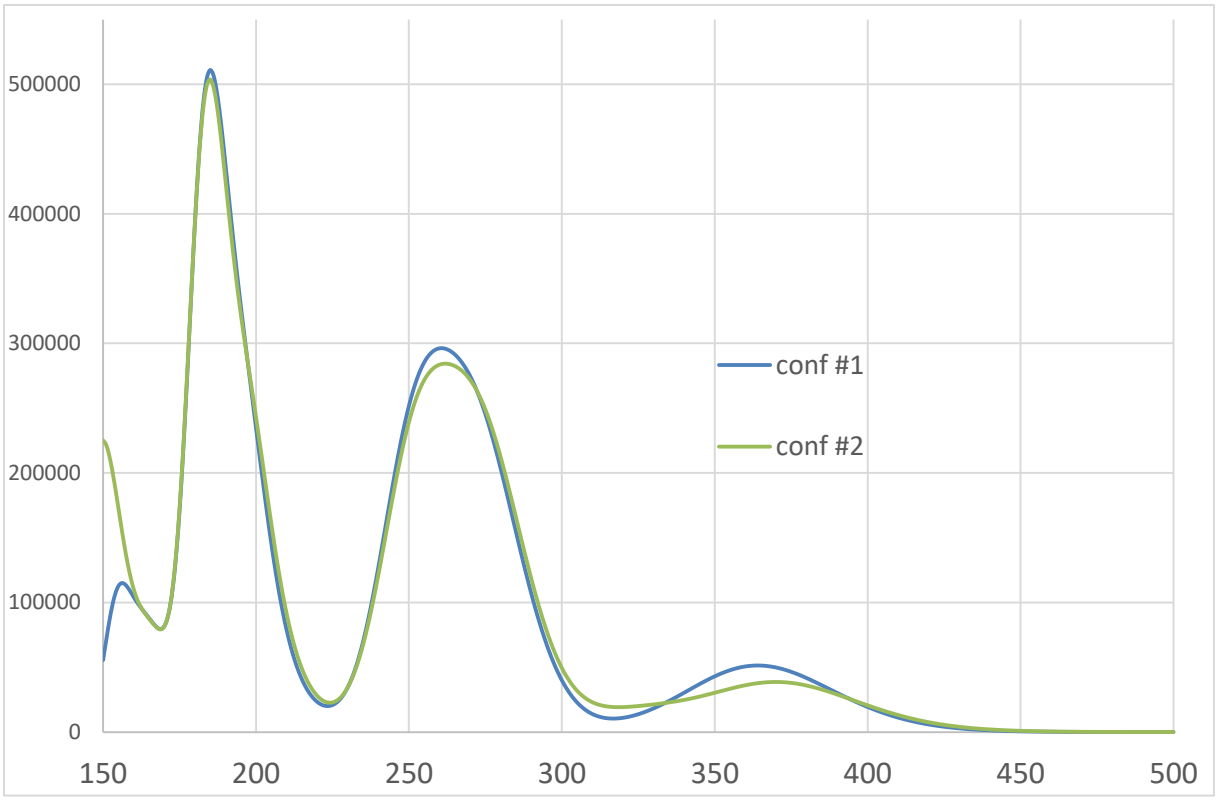

Figure S36. UV-Vis spectra calculated for individual conformers of **2**.

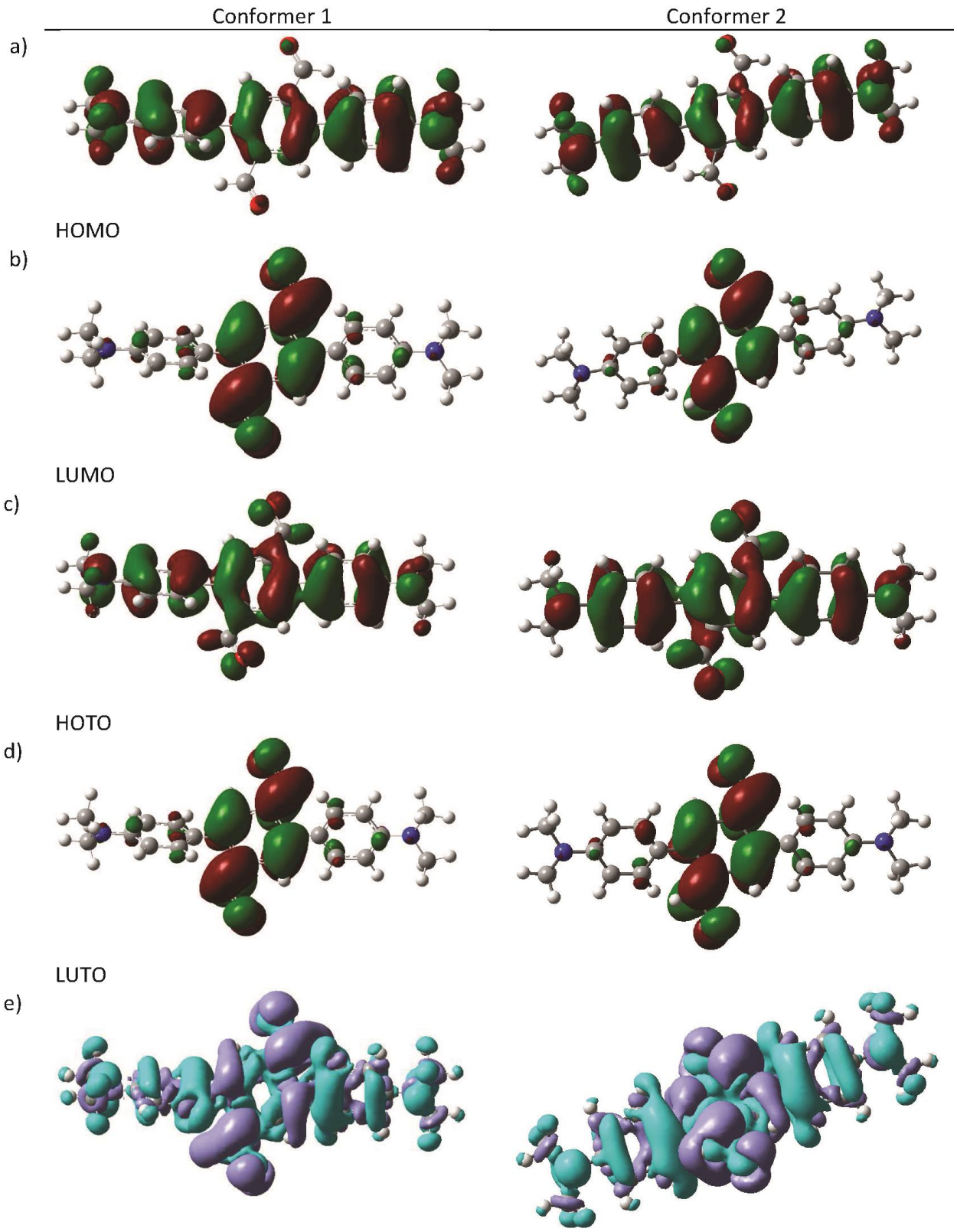

Figure S37. Molecular orbitals: a) HOMO; b) LUMO) and natural transition orbitals: c) HOTO; d) LUTO) for individual conformers of **2**. e) Electron difference density between the first excited state (blue) and the ground state (greenish) for individual conformers of **2**.

Single-crystal X-ray analysis

Crystals of compounds **1** and **2** suitable for X-ray structural analysis were obtained by slow evaporation of solvent. For compound **1**, depending on the used solvent, different crystal phases were obtained: **1α**: chloroform/dioxane 1:1; **1β**: chloroform/diethyl ether 1:1; **1γ**: chloroform/ethanol 1:1; **1δ**: chloroform/toluene 1:1. Crystals of compound **2** were obtained by crystallization from diethyl ether.

The diffraction data for crystals of **1** and **2** were collected at 100 K with a D8 QUEST system equipped with a Microfocus source Incoatec ImS DII (Cu, λ = 1.54184 Å). The frames were integrated with the Bruker SAINT software package using a narrow-frame algorithm (Bruker AXS LLC, 2019; SAINT V8.40B).[17] Data were corrected for absorption effects using the Multi-Scan method (SADABS). For **1γ,** data were collected at 100K with a Rigaku XtaLAB Synergy-R diffractometer (λ = 1.54184 Å). The intensity data were collected and processed using CrysAlis PRO software (Rigaku OD, version 1.171.43.143a).

Direct methods with the program solved all crystal structures SHELXT 2018/2[18] and refined by full-matrix least-squares method on F^2 with SHELXL 2018/3.[19] The carbon-bound hydrogen atoms were refined as riding on their carriers, and their displacement parameters were set equal to 1.5Ueq(C) for the methyl groups and 1.2Ueq(C) for the remaining H atoms.

A summary of the crystallographic data and refinements details is given in Table S4. Molecular graphics were generated with Olex2[20] and Mercury 2024.3.1 software.[21] Molecular structures of compounds **1** and **2** with atomic displacement ellipsoids are shown in Figures S38-S42.

CCDC 2487783-2487787 contains the supplementary crystallographic data for this paper. These data can be obtained free of charge via www.ccdc.cam.ac.uk/data_request/cif, or by emailing data_request@ccdc.cam.ac.uk, or by contacting The Cambridge Crystallographic Data Centre, 12 Union Road, Cambridge CB2 1EZ, UK; fax: +44 1223 336033.

Table S9. Selected crystal data and structure refinement details for crystals of compounds **1** and **2**

	1α	**1β**	**1γ**	**1δ**	**2**
CCDC number	**2487783**	**2487784**	**2487785**	**2487786**	**2487787**
Crystal data					
Chemical formula	$C_{44}H_{32}N_2O_2 \cdot C_4H_8O_2$		$C_{44}H_{32}N_2O_2$		$C_{24}H_{24}N_2O_2$
M_r					372.45
Crystal system, space group	Triclinic, $P\bar{1}$	Monoclinic, $P2_1/c$	Triclinic, $P\bar{1}$	Triclinic, $P\bar{1}$	Monoclinic, $P2_1/n$
Temperature (K)	100	100	100	100	100
a, *b*, *c* (Å)	7.7428 (8), 9.5268 (13), 14.902 (3)	9.6128 (6), 40.608 (2), 8.8896 (6)	7.74122 (16), 9.9660 (2), 20.5516 (5)	7.7445 (15), 9.953 (2), 21.129 (5)	11.7252 (7), 7.4302 (4), 22.1775 (13)
α, β, γ (°)	92.387 (10), 94.264 (9), 111.842 (7)	114.670 (4)	90.722 (2), 91.263 (2), 93.1373 (18)	76.392 (15), 89.979 (18), 86.844 (13)	96.807 (3)
V (Å^3)	1014.6 (3)	3153.4 (3)	1582.62 (7)	1580.5 (6)	1918.50 (19)
Z	1	4	2	2	4
Radiation type	Cu *K*α	Cu *K*α	Cu *K*α	Cu *K*α	Cu *K*α
□ (mm^{-1})	0.68	0.63	0.62	0.62	0.65
Data collection					
Absorption correction	Multi-scan	Multi-scan	Multi-scan	Multi-scan	Multi-scan
T_{min}, T_{max}	0.608, 0.754	0.564, 0.754	0.900, 1.000	0.675, 0.754	0.774, 1.000
No. of measured, independent and observed [$I > 2\sigma(I)$] reflections	3554, 3554, 2370	43575, 5385, 3901	23113, 5777, 5167	66416, 6452, 5224	25545, 3787, 2834
R_{int}	0.12	0.101	0.027	0.091	0.065
$(\sin\theta/\lambda)_{max}$ (Å^{-1})	0.619	0.596	0.602	0.631	0.619
Refinement					
$R[F^2 > 2\sigma(F^2)]$, $wR(F^2)$, *S*	0.116, 0.348, 1.24	0.059, 0.150, 1.08	0.045, 0.125, 1.03	0.073, 0.193, 1.07	0.048, 0.139, 1.06
No. of reflections	3554	5385	5777	6452	3787
No. of parameters	327	434	433	509	258
No. of restraints	72			17	
$\Delta\rho_{max}$, $\Delta\rho_{min}$ (e Å^{-3})	0.47, -0.44	0.26, -0.20	0.32, -0.35	0.62, -0.34	0.41, -0.24

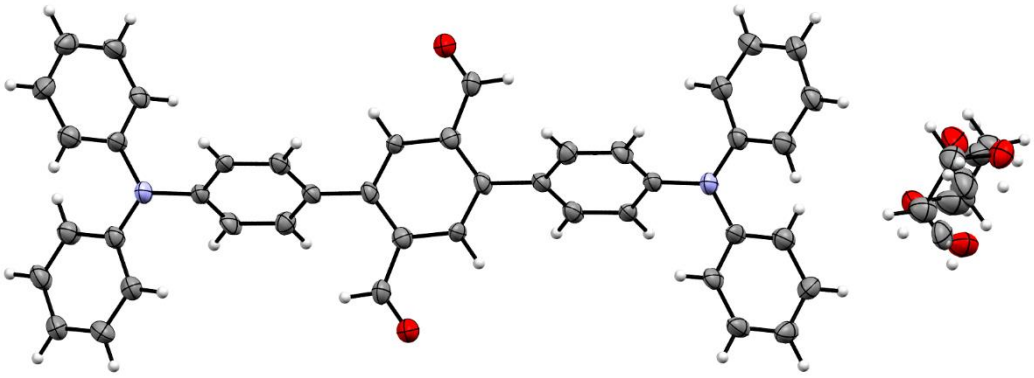

Figure S38. Molecular structure of **1α**.

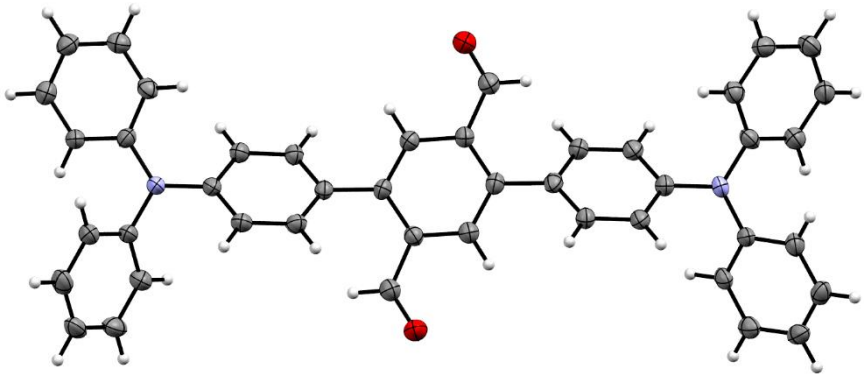

Figure S39. Molecular structure of **1β**.

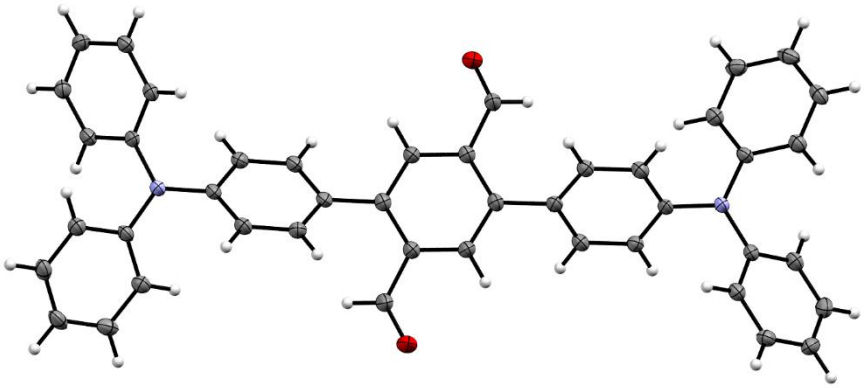

Figure S40. Molecular structure of **1γ**.

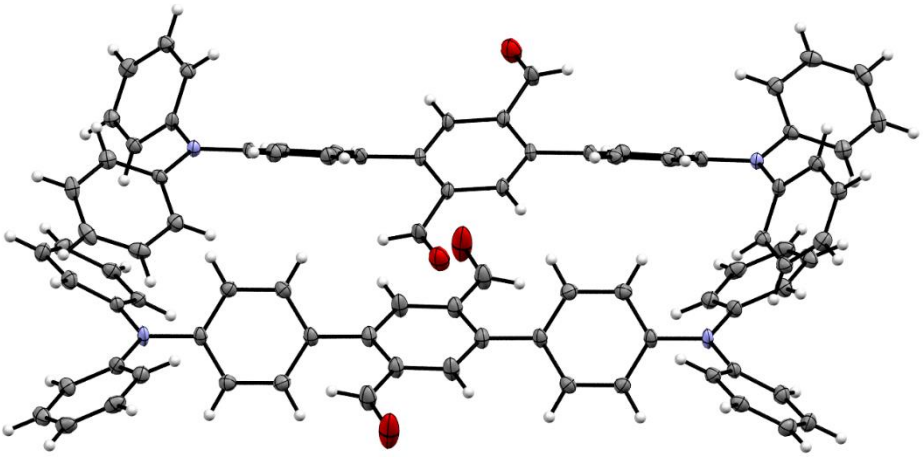

Figure S41. Molecular structure of **1δ**.

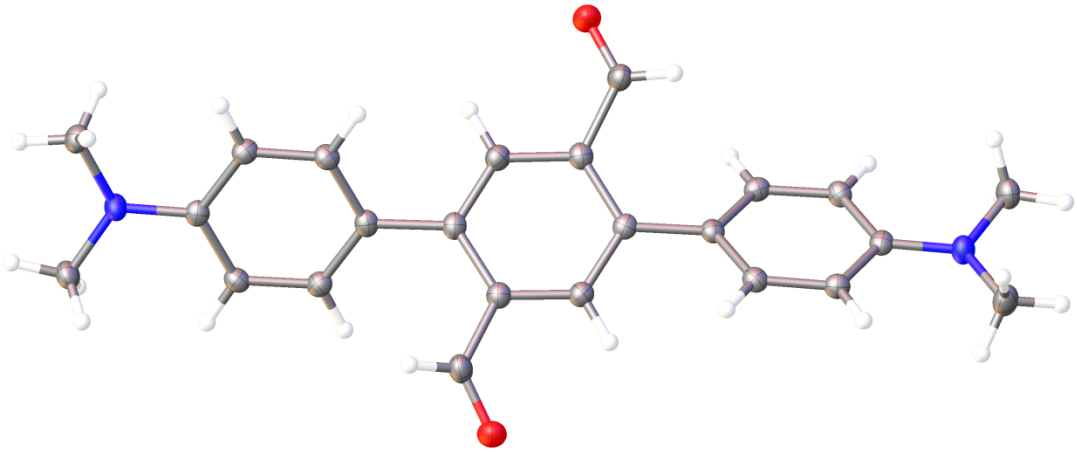

Figure S42. Molecular structure of **2**.

Table S10. Selected geometrical parameters for the molecule of compound **1** in different polymorphic structures, and for molecule **2**.

	β	*σ*	σ^R
1α	3.76	46.06	
1β	-1.05	50.88	-51.51
1γ	-83.56	-44.83	-42.30
$1\delta_1$	-5.72	45.65	
$1\delta_2$	-2.14	42.55	
2	-76.51	-36.83	-42.91

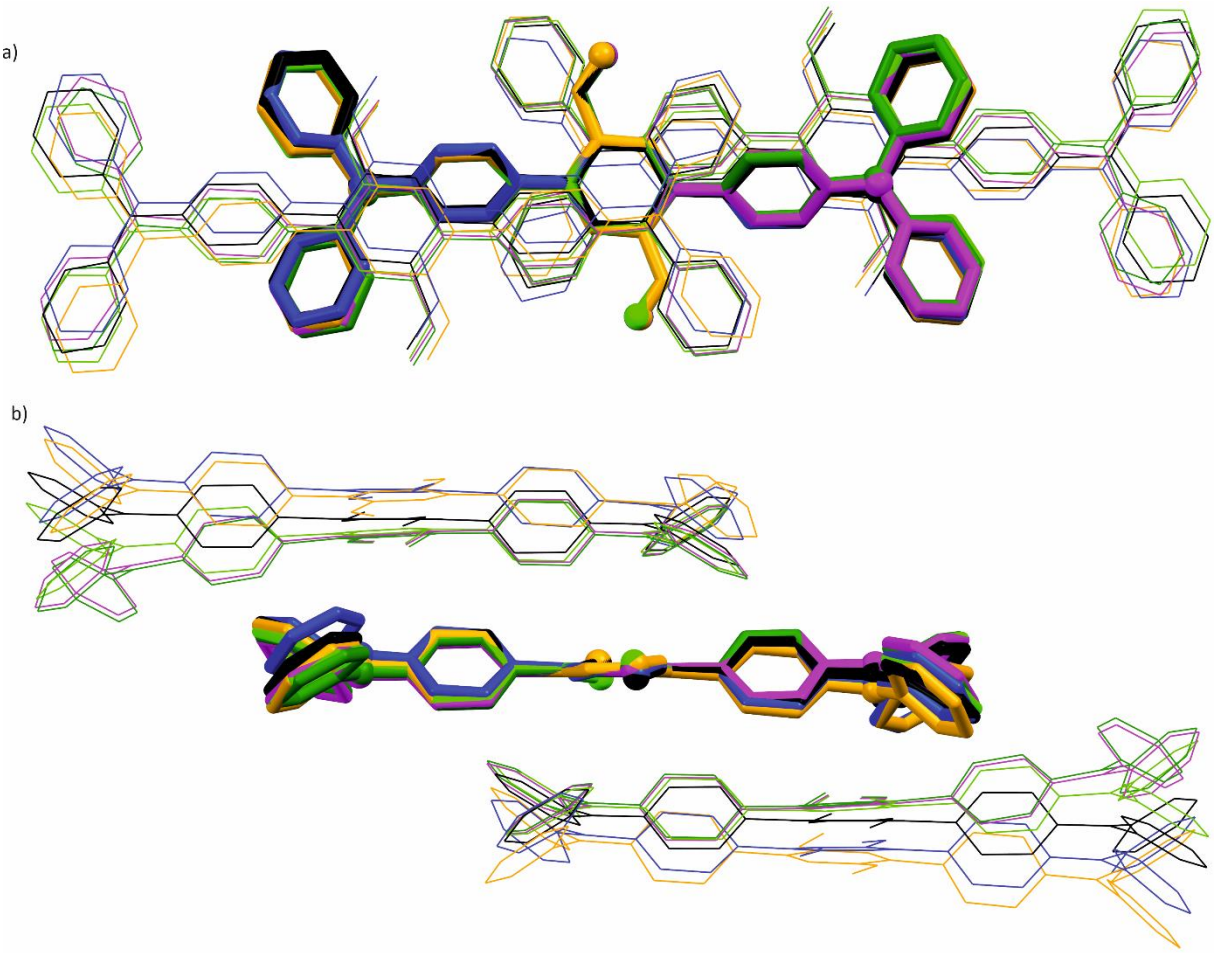

Figure S43. Comparison of trimolecular fragments of stacks in the crystal structure (black) of **1α** and optimized by various methods (yellow – B3LYP; light green - M06L; violet - B3LYP-GD3BJ; blue - APF; dark green -APFD): a) top and b) side view.

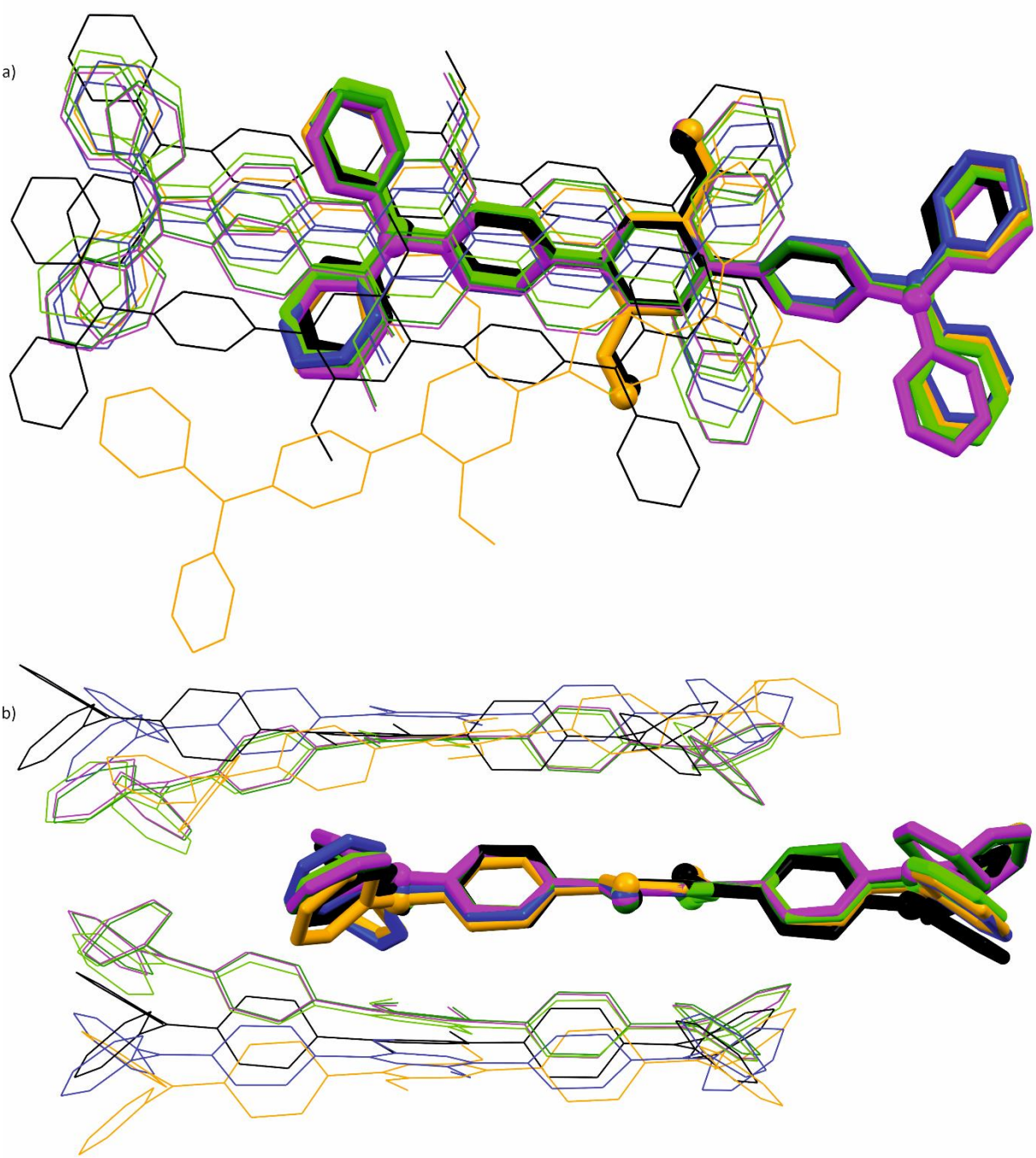

Figure S44. Comparison of trimolecular fragments of stacks in the crystal structure (black) of **1β** and optimized by various methods (yellow – B3LYP; light green - M06L; violet - B3LYP-GD3BJ; blue - APF; dark green -APFD): a) top and b) side view.

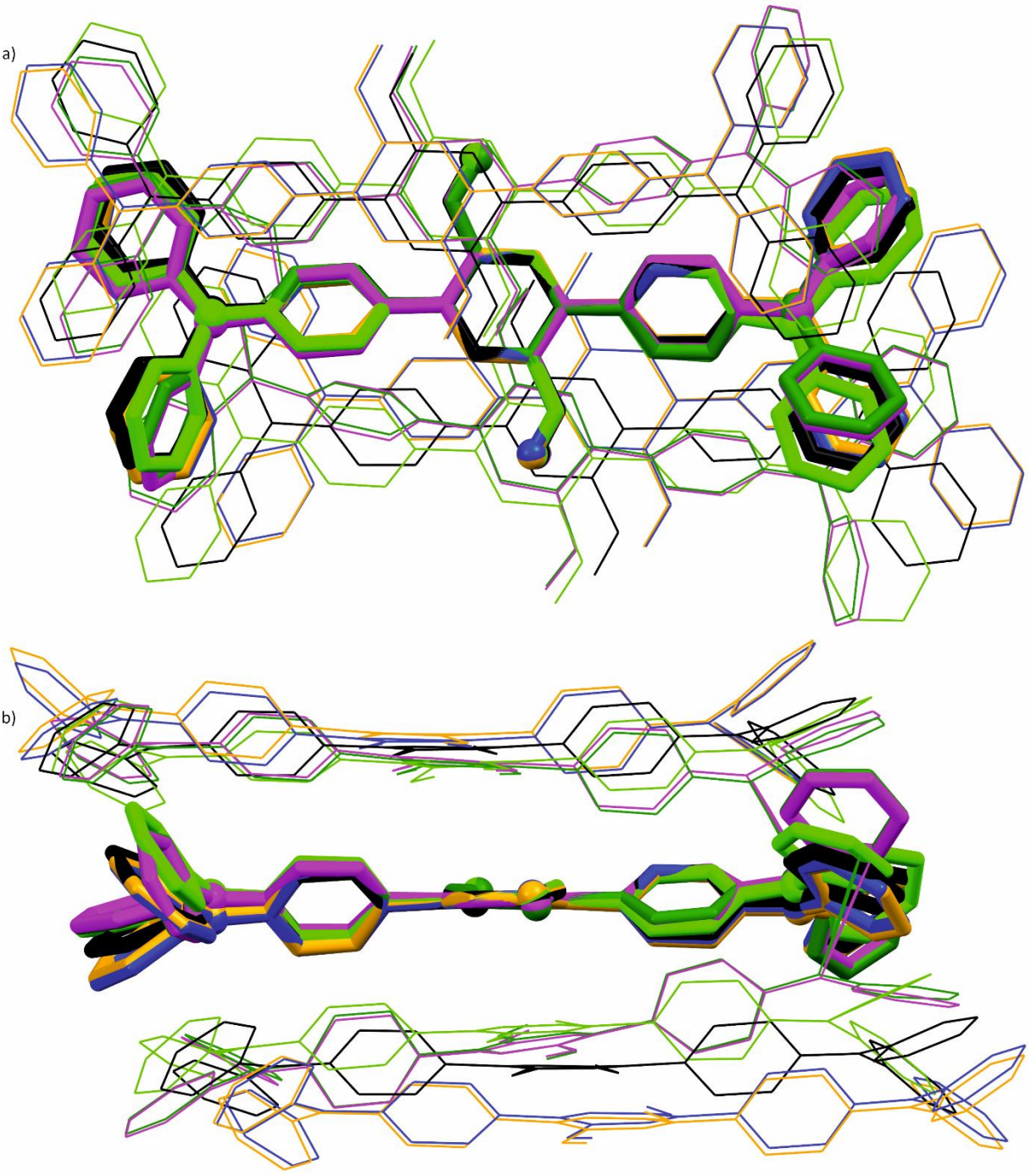

Figure S45. Comparison of trimolecular fragments of stacks in the crystal structure (black) of **1γ** and optimized by various methods (yellow – B3LYP; light green - M06L; violet - B3LYP-GD3BJ; blue - APF; dark green -APFD): a) top and b) side view.

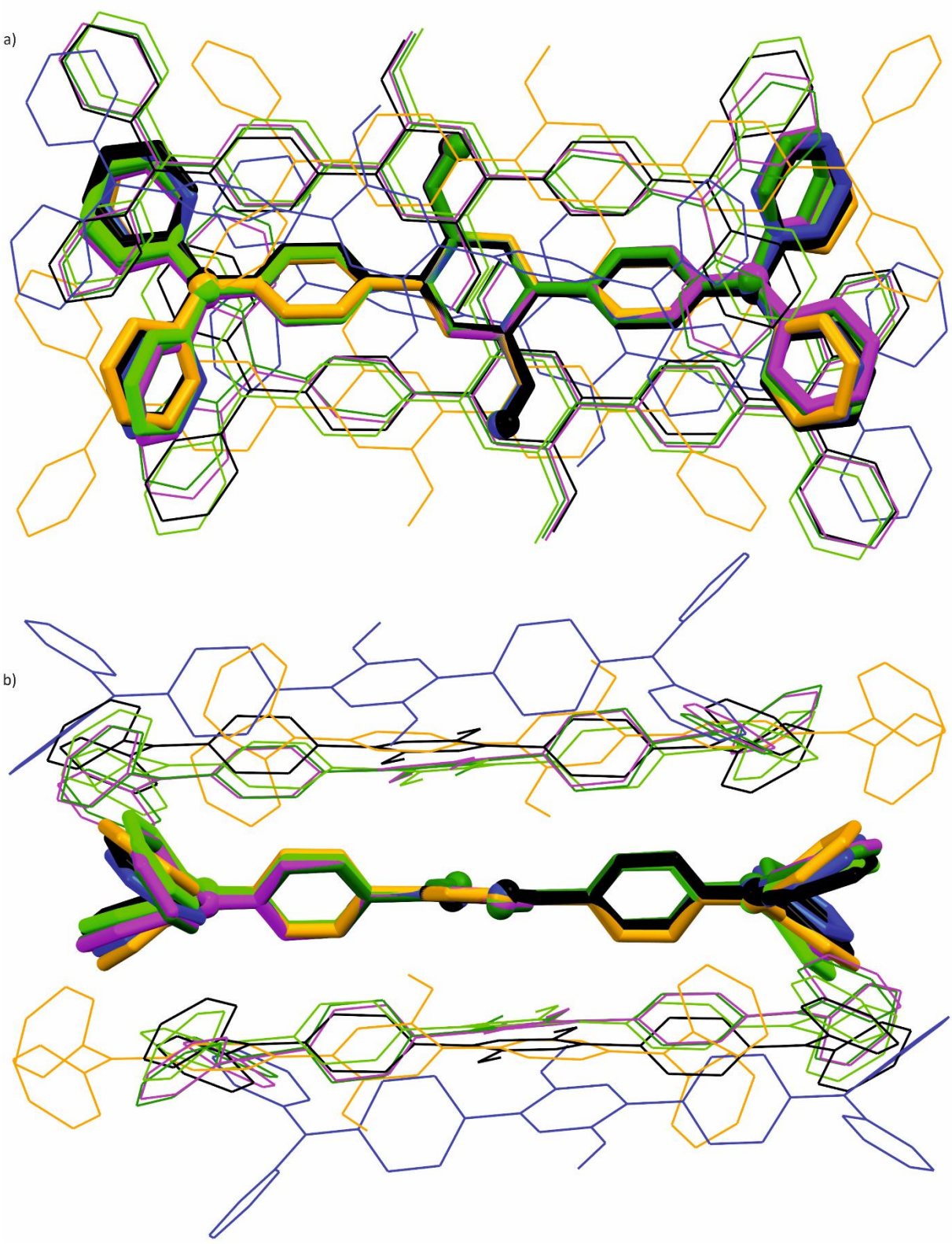

Figure S46. Comparison of trimolecular fragments of stacks in the crystal structure (black) of **1δ** and optimized by various methods (yellow – B3LYP; light green - M06L; violet - B3LYP-GD3BJ; blue - APF; dark green -APFD): a) top and b) side view.

Powder X-ray analysis

Powder patterns were registered with four-circle D8 QUEST system equipped with a Microfocus source Incoatec ImS DII using Cu Kα radiation (λ=1.54184 Å). A 0.2 mm pinhole collimator was used and the detector was set at 100 mm from the sample. The exposure time was fixed to 300 second per scan and images were collected with a 300 degrees phi rotation.

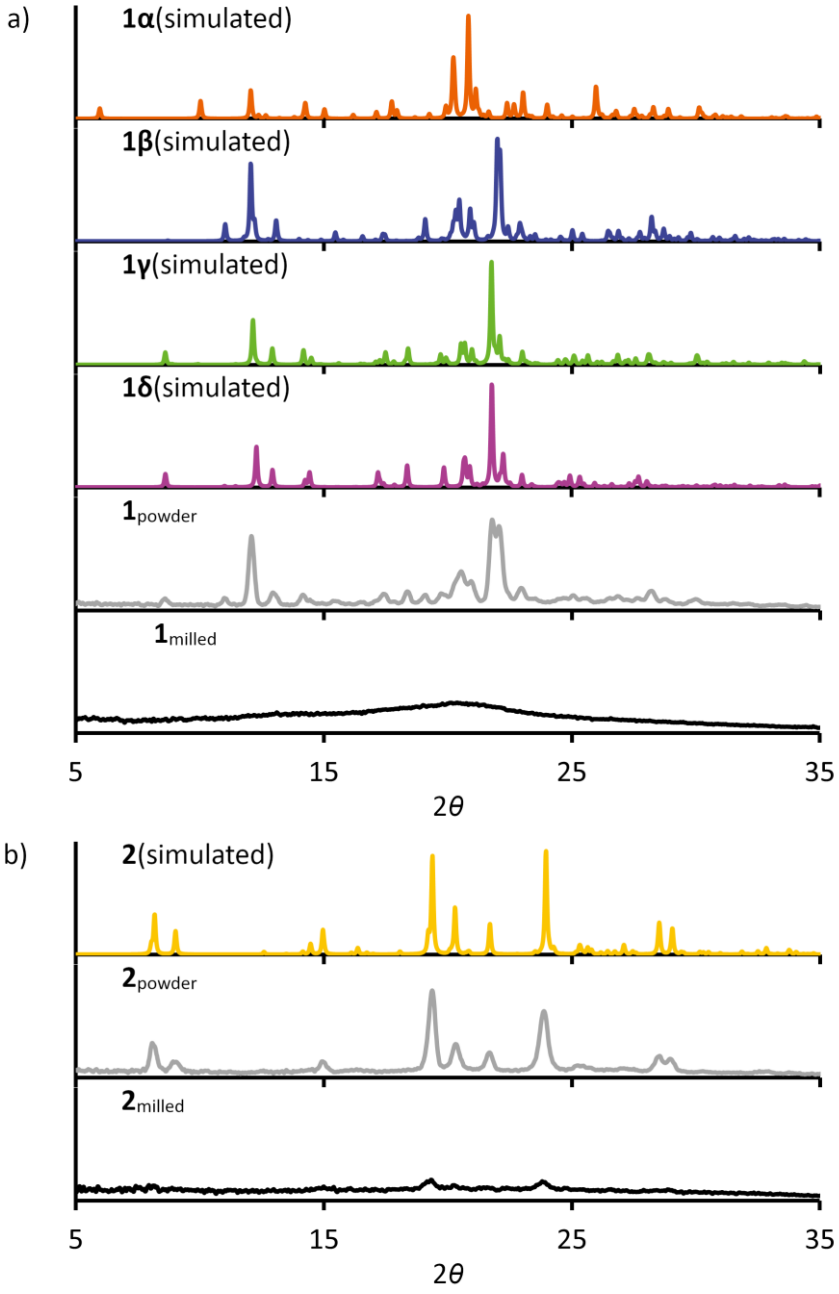

Figure S47. Comparison of powder X-ray diffraction patterns for compounds a) **1**; b) **2**.

References

[1] N. Prusinowska, M. Bardziński, A. Janiak, P. Skowronek and M. Kwit, *Chem. Asian J.*, 2018, **13**, 2691.
[2] Z. Zhong, X. Zhu, X. Wang, Y. Zheng, S. Geng, Z. Zhou, Xin J. Feng, Z. Zhao and H. Lu, *Adv. Funct. Mater.*, 2022, **32**, 2112969.
[3] The procedure is based on the work of C. Liu, Q. Ni and J. Qiu, *Eur. J. Org. Chem.*, 2011, 3009.
[4] G. Y. Ryu, S. G. Lee, S. E. Shin, J. J. Park, S. Park and D. M. Shin, *J. Nanosci. Nanotechnol.*, 2010, 6805.
[5] C. Liu, Q. Ni and J. Qiu, *Eur. J. Org. Chem.*, 2011, 3009.
[6] Scigress, version 2.5; Fujitsu Ltd.: Tokyo, Japan, 2013.
[7] A. D. Becke, *J. Chem. Phys*., 1993, **98**, 5648.
[8] Gaussian 16, Revision C.01, M. J. Frisch, G. W. Trucks, H. B. Schlegel, G. E. Scuseria, M. A. Robb, J. R. Cheeseman, G. Scalmani, V. Barone, G. A. Petersson, H. Nakatsuji, X. Li, M. Caricato, A. V. Marenich, J. Bloino, B. G. Janesko, R. Gomperts, B. Mennucci, H. P. Hratchian, J. V. Ortiz, A. F. Izmaylov, J. L. Sonnenberg, D. Williams-Young, F. Ding, F. Lipparini, F. Egidi, J. Goings, B. Peng, A. Petrone, T. Henderson, D. Ranasinghe, V. G. Zakrzewski, J. Gao, N. Rega, G. Zheng, W. Liang, M. Hada, M. Ehara, K. Toyota, R. Fukuda, J. Hasegawa, M. Ishida, T. Nakajima, Y. Honda, O. Kitao, H. Nakai, T. Vreven, K. Throssell, J. A. Montgomery, Jr., J. E. Peralta, F. Ogliaro, M. J. Bearpark, J. J. Heyd, E. N. Brothers, K. N. Kudin, V. N. Staroverov, T. A. Keith, R. Kobayashi, J. Normand, K. Raghavachari, A. P. Rendell, J. C. Burant, S. S. Iyengar, J. Tomasi, M. Cossi, J. M. Millam, M. Klene, C. Adamo, R. Cammi, J. W. Ochterski, R. L. Martin, K. Morokuma, O. Farkas, J. B. Foresman and D. J. Fox, Gaussian, Inc., Wallingford CT, 2019.
[9] S. Grimme, *J. Chem. Phys.*, 2006, 034108.
[10] T. Yanai, D. Tew and N. Handy, *Chem. Phys. Lett.*, 2004, **393**, 51.
[11] Y. Zhao and D. G. Truhlar, *J. Phys. Chem.*, 2006, 5121.
[12] Y. Zhao and D. G. Truhlar, *Theor. Chem. Acc.*, 2008, **120**, 215.
[13] R. L. Martin, *J. Chem. Phys.*, 2003, **118**, 4775.
[14] GaussView 6.1.1 Semichem, Inc. 2000-2019.
[15] A. Austin, G. Petersson, M. J. Frisch, F. J. Dobek, G. Scalmani and K. Throssell, *J. Chem. Theory and Comput.*, 2012, **8**, 4989.
[16] S. Grimme, S. Ehrlich and L. Goerigk, *J. Comp. Chem*., 2011, **32**, 1456.
[17] L. Krause, R. Herbst-Irmer, G. M. Sheldrick and D. Stalke, *J. Appl. Crystallogr.*, 2015, **48**, 3.
[18] G. M. Sheldrick, *Acta Cryst*., 2015,. **A71**, 3.
[19] G. M. Sheldrick, *Acta Cryst.*, 2015, **C71**, 3.
[20] O. V. Dolomanov, L. J. Bourhis, R. J. Gildea, J. A. K. Howard and H. Puschmann, *J. Appl. Crystallogr.*, 2009, **42**, 339.
[21] C. F. Macrae, I. Sovago, S. J. Cottrell, P. T. A. Galek, P. McCabe, E. Pidcock , M. Platings, G. P. Shields, J. S. Stevens, M. Towler and P. A. Wood, *J. Appl. Crystallogr.*, 2020, **53**, 226.